

Topical Review: The rise of Klein tunneling in low-dimensional materials and superlattices

Yonatan Betancur-Ocampo,^{1,*} Guillermo Monsivais,^{1,†} and Vít Jakubský^{2,‡}

¹*Instituto de Física, Universidad Nacional Autónoma de México, Ciudad de México, Mexico*

²*Nuclear Physics Institute, Czech Academy of Science, 250 68 Řež, Czech Republic*

We review recent advances in Klein and anti-Klein tunneling in one- and two-dimensional materials. Using a general tight-binding framework applied to multiple periodic systems, we establish the criteria for the emergence of Klein tunneling based on the conservation of an effective reduced pseudospin. The inclusion of higher-order terms in the wave vector leads to nontrivial matching conditions for wave scattering at interfaces. We further examine the emergence of multiple types of Klein tunneling in two-dimensional materials beyond graphene, including phosphorene and borophene, as well as in one-dimensional systems such as Su-Schrieffer-Heeger lattices. Finally, we discuss how these tunneling phenomena can be tested in both synthesized and artificial lattices, including elastic metamaterials, optical, photonic, phononic, and superconducting platforms, demonstrating the universality of Klein tunneling across different wave natures and length scales.

INTRODUCTION: OVERVIEW ON THE ORIGIN OF KLEIN TUNNELING

Since 1929, Oskar Klein predicted one of the most outstanding tunneling phenomena in the context of high-energy physics [1]. This phenomenon, called today Klein tunneling, consists of a non-resonant perfect transmission of massless particles through a gradient electrostatic potential, where the kinetic energy can be less than the potential height [2–4]. Such an effect does not necessarily involve crossing classical forbidden regions via evanescent waves, like a Landauer-Zener tunneling in condensed matter [5, 6]. Interestingly, Klein tunneling has not been tested in high-energy physics experiments so far. However, the first experimental realization of Klein tunneling was performed in condensed matter with the discovery of graphene [4, 7]. In contrast to the Klein tunneling originally predicted in high-energy physics, this perfect transmission emerges in graphene within a low-energy regimen, when electrons pass from one band (conduction or valence band) to another under normal incidence, conserving an associated pseudospin lattice [2–4]. It is worth noting that Klein tunneling is not exclusive to spin-1/2 charged particles that normally impinge on an external electrostatic potential, as it is possible to realize analogues of Klein tunneling for phonons or photons in artificial lattices [8–11].

Klein tunneling can also occur for massive particles with enlarged pseudospin beyond spin 1/2 and independent of the incidence angle, effect called as super-Klein tunneling [10–42]. This omnidirectional perfect transmission is performed in two-dimensional lattices with unit cells containing three atoms, among them: α - τ_3 lattices [28, 41, 43–53], Lieb lattices [5, 32, 54–85], and honeycomb superlattices [15, 86–93]. In such systems, electrons behave as particles with pseudospin-one, where a flat band lies between two dispersive bands [18, 94, 95]. The study of materials with flat bands has increased recently due to its outstanding effects on electronic proper-

ties [45, 96–104]. Super-Klein tunneling has recently been observed recently in acoustic experiments with triangular lattices of Willis resonant scatterers [10] and phononic Lieb lattice [11].

Several variants of Klein tunneling have been identified. One notable example is anomalous Klein tunneling, which corresponds to a non-resonant perfect transmission with a pronounced angular dependence. This phenomenon arises in two-dimensional materials such as borophene 8-pmmn, uniaxially strained graphene [31, 105–107], and photonic graphene, the latter of which has been realized experimentally [9]. In Kekulé graphene superlattices, a different type of Klein tunneling is predicted, where perfect transmission is accompanied by a valley flip [108]. The opposite phenomena, known as anti-Klein tunneling, corresponds to a perfect backscattering under normal incidence, which has been predicted in bilayer graphene and checkerboard lattices [21, 109, 110]. The omnidirectional version named anti-super-Klein tunneling has been studied in phosphorene and few-layer black phosphorus [111–114]. Beyond the Klein tunneling, more phenomena with flat bands have been predicted, such as Andreev reflection [2, 33, 110, 115], chiral magnons [116], topological charge pump [96], super skew scattering [45], Seebeck and Nernst effects [29], enhanced magneto-optical effect [22], Anderson localization [26], and electron-beam collimation [17, 27]. The wide variety of predicted and observed Klein tunneling phenomena is derived from the unusual electronic and transport properties of novel low-dimensional materials.

Another related topic is electron optics, which arises from the wave-particle duality with outstanding technological applications, such as the electron microscope. The rise of two-dimensional materials has recently given electron optics a new avenue. The experimental observation of negative refraction in graphene paves the way for the design of Veselago lenses [117, 118], since electrons are refracted according to a generalized Snell's law, where gating serves as the refractive index to tune the

electrostatic potential and Fermi level [3, 91, 111, 118–126]. In this way, electron optics enables the simulation of refraction phenomena, such as light propagation through metamaterials [71, 127–129]. Controlling electron flow in two-dimensional materials can lead to the proposal of a series of nanodevices, among them super-lenses [19, 31, 122, 130–135], valley beam splitters and filters [24, 108, 136–152], collimators [27, 91, 107, 153–155], fiber-optic guidings [112, 139, 156–160], interferometers [161, 162], reflectors [2, 33, 43, 72, 107, 110, 111, 163–168], and use the valley degree of freedom as conveyor of quantum information [108, 136, 142, 151, 169]. Klein and anti-Klein tunneling may help to improve the efficiency of these electron optics tools.

Recently, one-dimensional lattices have been widely investigated in artificial systems using effective models based on tight-binding approach [25, 101, 170–197], where the main study is focused on topological phase transitions [198–200]. Nevertheless, Klein tunneling has been explored scarcely in 1D chains due to the difficulty of creating an abrupt *pn* junction in polyacetylene and other molecules to test perfect tunneling. Artificial lattices enable us to explore atypical Klein tunneling in different branches of physics, such as optics, acoustics, and elastic waves.

In this Review, we analyze the various versions of Klein tunneling from a general perspective. For that, the first section is dedicated to the application of the tight-binding approach to a crystal of n atoms in the unit cell, where a general Bloch Hamiltonian is derived. This framework is employed in the analysis of Klein tunneling of a rectangular electric barrier. The continuity of the wave functions of Bloch Hamiltonian is obtained from general considerations in the second section, because the Bloch Hamiltonian involves higher-order terms in the wave vector \mathbf{k} . In the third and fourth sections, we establish the analogs of Fresnel coefficients in condensed matter and metamaterials by applying the continuity wave function for step potentials, barriers, and stratified media under the reformulation of the transfer matrix method.

In the fifth section, we derive the laws of electron optics in anisotropic media from the conservation of energy and linear momentum within the framework of a Dirac-type Hamiltonian. The sixth section is devoted to the study of super-Klein tunneling in pseudo-spin one systems and in the presence of a periodic chain of scatterers, using the formalism of supersymmetric quantum mechanics. From the previous theoretical frameworks, the seventh section analyzes the emergence of Klein and anti-Klein tunneling. Several manifestations of these effects are examined in two-dimensional materials such as graphene, borophene, phosphorene, as well as in artificial crystals including phononic Lieb and dice lattices.

TIGHT BINDING APPROACH OF LOW-DIMENSIONAL LATTICES

The tight-binding approach is based on the consideration of a set of atoms in the molecule, nanostructure, polymeric chain, or d -dimensional crystal for the latter electron in the atomic orbital [55, 175, 176, 181, 183, 201–209]. This electron interacts with the total energy potential due to the other electrons and nuclear ions. Each atom in the site is located at the minimum of this potential, like a quantum well. Therefore, the electron is confined in the potential well with the possibility to hop to another atom site across the tunnel effect. This scenario is not exclusive to electrons in molecules or crystals. The undulatory behavior of the confined electron in the potential well can also be emulated by other types of waves, such as elastic, electromagnetic, or sound waves, which are resonating within a cavity. If the cavities possess sidewalls with the possibility of leakage, the waves escape across evanescent modes to arrive at the neighborhood of the other cavity. In this way, artificial molecules, nanostructures, and d -dimensional crystals can be emulated [9, 71, 170, 172, 175, 176, 178, 180, 193, 210–218].

For the particular situation of describing the electron propagation in a crystal, the wave function is

$$\psi_j(\mathbf{r}, \mathbf{k}) = \sum_{\mathbf{R}_\ell} e^{i\mathbf{k}\cdot(\mathbf{R}_\ell + \boldsymbol{\delta}_j)} \phi_j(\mathbf{r} - \boldsymbol{\delta}_j - \mathbf{R}_\ell), \quad (1)$$

which satisfies the Bloch theorem, where \mathbf{k} is the wave vector, the index $j = 1, 2, \dots, n$ indicates the position inside the unit cell, and \mathbf{R}_ℓ are lattice vectors, the index ℓ labels the unit cell positions. The vectors $\boldsymbol{\delta}_j$ correspond to the atomic positions within the unit cell. The function ϕ_j is the outer orbital of the j -th atom. In the following, we consider only a piece of crystal of N unit cells and suppose that the expression in Eq. (1) remains valid approximately, where ℓ goes from 1 to N .

To get the matrix representation of the TB Hamiltonian, we split the Hamiltonian in two parts

$$\hat{H} = \hat{H}_{\text{at}} + \hat{V}_{\text{cr}}, \quad (2)$$

where \hat{H}_{at} is the atomic Hamiltonian acting on the site j :

$$\hat{H}_{\text{at}}\phi_j(\mathbf{r}) = \epsilon_j\phi_j(\mathbf{r}) \quad (3)$$

and \hat{V}_{cr} is the electrostatic potential of the electron with the whole crystal. Therefore, the matrix elements are

$$H_{jm} = \int_V \psi_j^*(\mathbf{r})(\hat{H}_{\text{at}} + \hat{V}_{\text{cr}})\psi_m(\mathbf{r})dV. \quad (4)$$

Substituting the Bloch wave function of Eq. (1) in the H_{jm} elements, we have

$$H_{jm}(\mathbf{k}) = \sum_{\mathbf{R}'_\ell, \mathbf{R}_\ell} e^{i\mathbf{k}\cdot(\mathbf{R}_\ell - \mathbf{R}'_\ell + \boldsymbol{\delta}_m - \boldsymbol{\delta}_j)} \left[\epsilon_j W_{jm}^{\ell\ell'} + T_{jm}^{\ell\ell'} \right], \quad (5)$$

where we define

$$W_{jm}^{\ell\ell'}(\mathbf{R}_\ell) \equiv \int_V \phi_j^*(\mathbf{r} - \boldsymbol{\delta}_j - \mathbf{R}'_\ell) \phi_m(\mathbf{r} - \boldsymbol{\delta}_m - \mathbf{R}_\ell) dV, \quad (6)$$

which is the integral that quantifies the degree of overlapping of the orbital at the site j for the unit cell ℓ with respect to another located at the site m in the unit cell ℓ' . While the element

$$T_{jm}^{\ell\ell'} = \int_V \phi_j^*(\mathbf{r} - \boldsymbol{\delta}_j - \mathbf{R}'_\ell) V_{cr}(\mathbf{r}) \phi_m(\mathbf{r} - \boldsymbol{\delta}_m - \mathbf{R}_\ell) dV \quad (7)$$

is the hopping integral and must be interpreted as a probability amplitude of the electron that hops from the atom j in the unit cell ℓ to the atomic site m in the unit cell ℓ' .

The quantity $\Delta\mathbf{R} = \mathbf{R}_\ell - \mathbf{R}'_{\ell'}$ is also a lattice vector, and the sum in Eq. (5) has N repeated terms due to the N unit cells in the crystal. Therefore, the TB Hamiltonian can be written as

$$H_{jm}(\mathbf{k}) = N(\epsilon_j W_{jm}(\mathbf{k}) + T_{jm}(\mathbf{k})) = N h_{jm}(\mathbf{k}). \quad (8)$$

The overlap matrix elements are

$$W_{jm}(\mathbf{k}) = \sum_{\Delta\mathbf{R}} w_{jm}^{(\Delta\mathbf{R})} e^{i\mathbf{k}\cdot(\Delta\mathbf{R} + \boldsymbol{\delta}_{mj})}, \quad (9)$$

with $\boldsymbol{\delta}_{mj} = \boldsymbol{\delta}_m - \boldsymbol{\delta}_j$ and

$$w_{jm}^{(\Delta\mathbf{R})} = \int_V \phi_j^*(\mathbf{r}) \phi_m(\mathbf{r} - \Delta\mathbf{R} - \boldsymbol{\delta}_{mj}) dV. \quad (10)$$

The hopping matrix elements are

$$T_{jm}(\mathbf{k}) = \sum_{\Delta\mathbf{R}} t_{jm}^{(\Delta\mathbf{R})} e^{i\mathbf{k}\cdot(\Delta\mathbf{R} + \boldsymbol{\delta}_{mj})}, \quad (11)$$

where the hopping parameter between the atoms with positions $\boldsymbol{\delta}_j$ and $\boldsymbol{\delta}_m + \Delta\mathbf{R}$ is

$$t_{jm}^{(\Delta\mathbf{R})} = \int_V \phi_j^*(\mathbf{r}) V(\mathbf{r}) \phi_m(\mathbf{r} - \Delta\mathbf{R} - \boldsymbol{\delta}_{mj}) dV. \quad (12)$$

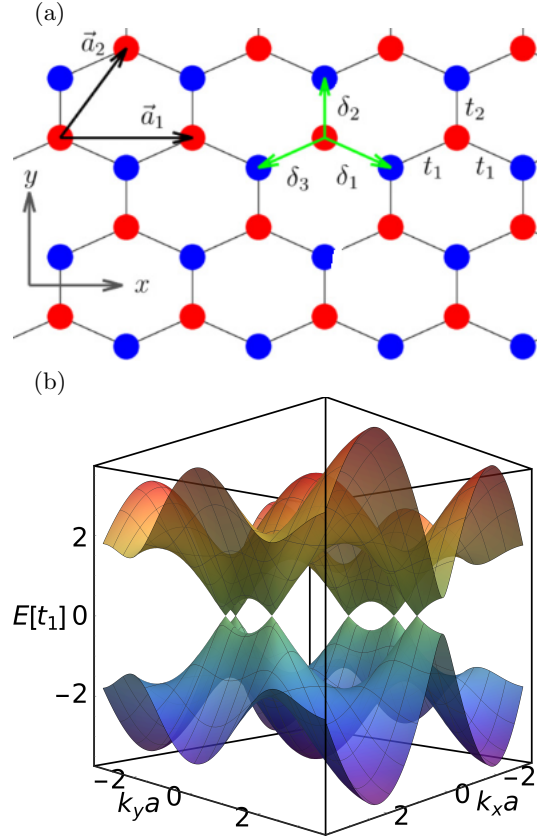


Figure 1. (a) Anisotropic hexagonal lattice that represents to strained graphene and simplified phosphorene structure, which is formed by two triangular sublattices. The arrows correspond to lattice vectors and nearest neighbors of atoms within the unit cell. The hopping parameters are t_1 and t_2 for quinoid deformation. (b) Electronic band structure with the values of $\epsilon_1 = \epsilon_2 = 0$, $t_1 = 1$, and $t_2 = 1.6$. The variation of hopping parameters can induce a gap opening for $t_2 \geq 2t_1$.

An approximation in the tight-binding approach is to neglect the overlap among atoms, where $W_{jm} \approx \delta_{jm}$, herein δ_{jm} is the Kronecker delta. Therefore, the effective TB Hamiltonian in Eq. (8) is

$$h_{jm}^{(TB)}(\mathbf{k}) \approx \epsilon_j \delta_{jm} + T_{jm}(\mathbf{k}). \quad (13)$$

It is also customary to retain the nearest neighbor interaction only; that is, the hopping amplitude $t_{jm}^{(\Delta\mathbf{R})}$ is set to zero for all non-nearest-neighbor sites.

While two-dimensional materials, such as strained graphene and phosphorene, as shown in Fig. 1(a), the Bloch Hamiltonian is obtained taking into account two atoms in the unit cell to nearest neighbors [31, 111, 112, 207, 209, 219–226]

$$H_{2D}(\mathbf{k}) = \begin{pmatrix} \epsilon_1 & \sum_{j=1}^3 t_j e^{-i\mathbf{k}\cdot\boldsymbol{\delta}_j} \\ \sum_{j=1}^3 t_j e^{i\mathbf{k}\cdot\boldsymbol{\delta}_j} & \epsilon_2 \end{pmatrix}, \quad (14)$$

where we have introduced the following change of notation $\delta_{1j} \rightarrow \delta_j$ and $t_{1j} \rightarrow t_j$ with $j = 1, 2$ and 3 for the nearest neighbor positions and hopping parameters, respectively. These relative positions without deformation are given by $\delta_1 = (\sqrt{3}/2, -1/2)a$, $\delta_2 = (0, 1)a$, and $\delta_3 = (-\sqrt{3}/2, -1/2)a$, with $a = 0.142$ nm the bond length of graphene [227]. The diagonalization of the Bloch Hamiltonian (14) for the anisotropic hexagonal lattice gives us the electronic band structure, as seen in Fig. 1(b).

On the other hand, we can consider a chain with three atoms in the unit cell, see Fig. 2(a), which is known as the bearded Su-Schrieffer-Heeger (SSH) lattice [181, 189, 195]

$$h(\mathbf{k}) \approx \begin{pmatrix} \epsilon_1 & T_{12}(\mathbf{k}) & T_{13}(\mathbf{k}) \\ T_{12}^*(\mathbf{k}) & \epsilon_2 & T_{23}(\mathbf{k}) \\ T_{13}^*(\mathbf{k}) & T_{23}^*(\mathbf{k}) & \epsilon_3 \end{pmatrix}, \quad (15)$$

where the functions $T_{ij}(\mathbf{k})$ are expressed in terms of hopping parameters to nearest neighbors

$$\begin{aligned} T_{12}(\mathbf{k}) &\approx t_{12}e^{i\mathbf{k}\cdot\delta_{21}} + t'_{12}e^{i\mathbf{k}\cdot\delta'_{21}}, \\ T_{13}(\mathbf{k}) &\approx t_{13}e^{i\mathbf{k}\cdot\delta_{13}} \\ T_{23}(\mathbf{k}) &\approx t_{23}e^{i\mathbf{k}\cdot\delta_{23}}. \end{aligned} \quad (16)$$

The expression $T_{12}(\mathbf{k})$ corresponds to the coupling between the atoms at sites 1 and 2. The coupling t_{12} reflects the hopping to the site 1 from the site 2 within the unit cell, whereas t'_{12} corresponds to the hopping from the site 2 to the adjacent cell. If the lattice is anisotropic, the parameters t_{12} and t'_{12} are different. The functions $T_{13}(\mathbf{k})$ and $T_{23}(\mathbf{k})$ corresponds to couplings within the unit cell, where t_{13} and t_{23} are the nearest-neighbor hoppings. In the bearded SSH lattice in Fig. 2(a), we set $\mathbf{k} = (k_x, 0)$ and the hopping parameters $t_{12} = t$, $t'_{12} = t'$, $t_{13} = h$, and $t_{23} = 0$. Fixing the relative position vectors $\delta_{21} \rightarrow \delta_3 = a_0(1, 0)$, $\delta'_{21} \rightarrow \delta_1 = a_0(-1, 0)$, and $\delta_{13} \rightarrow \delta_2 = a_0(0, 1)$, we obtain the simplified Hamiltonian

$$H_{1D}(k) = \begin{pmatrix} \epsilon_1 & te^{ika/2} + t'e^{-ika/2} & h \\ te^{-ika/2} + t'e^{ika/2} & \epsilon_2 & 0 \\ h & 0 & \epsilon_3 \end{pmatrix}. \quad (17)$$

This Hamiltonian has been used to study Klein tunneling in bearded SSH lattices [112]. The electronic band structure, obtained from the eigenenergies of the Hamiltonian in Eq. (17), depends on the choice of hopping parameters, as shown in Fig. 2(b).

Tuning the hopping parameters, for instance, with the application of strain on the material [31, 220, 223], is possible to change either smoothly or drastically the electronic and transport properties, and in some cases, the induction of topological phase transitions [228–230]. In

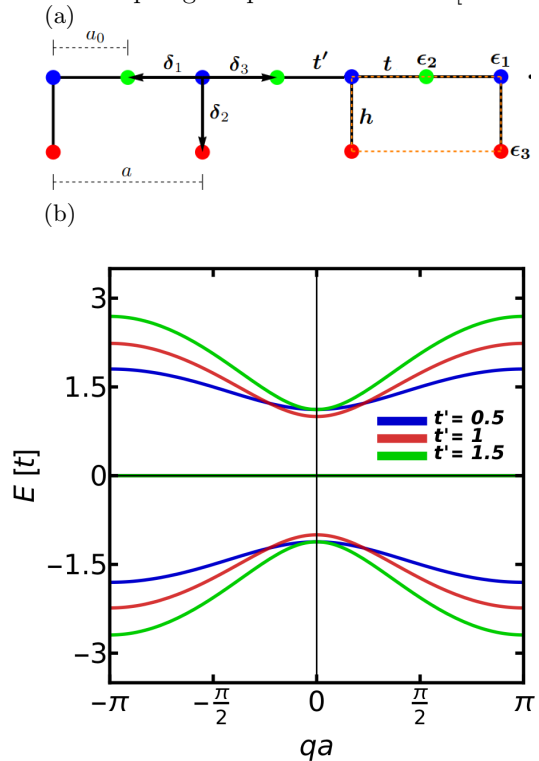


Figure 2. (a) Bearded Su-Schrieffer-Heeger lattice and (b) its electronic band structure with the set of onsite energies $\epsilon_1 = \epsilon_2 = \epsilon_3 = 0$ and hopping parameters $t = h = 1$, and $t' = 0.5, 1, 1.5$.

artificial systems, such as elastic metamaterials, the modulation of hopping parameters can be performed straightforwardly, where it is possible a great control in the phase transition [218, 231].

GENERAL MATCHING CONDITIONS OF WAVE FUNCTIONS FROM A BLOCH HAMILTONIAN

For interfaces in a material with abrupt changes in the electrostatic potential, the matching conditions are obtained by integrating the Schrödinger equation into a narrow range $(-\epsilon, \epsilon)$ around the abrupt jump in the electrostatic potential $V(x)$ at $x = 0$. Choosing as an example the Bloch Hamiltonian in Eq. (17) of the bearded SSH lattice, we get

$$\lim_{\epsilon \rightarrow 0} \int_{-\epsilon}^{\epsilon} [H(q) + V(x)] \Psi(x) dx = E \lim_{\epsilon \rightarrow 0} \int_{-\epsilon}^{\epsilon} \Psi(x) dx \quad (18)$$

$$\lim_{\epsilon \rightarrow 0} \int_{-\epsilon}^{\epsilon} \begin{pmatrix} \epsilon_1 + V(x) & \hat{g}^*(q) & h \\ \hat{g}(q) & \epsilon_2 + V(x) & 0 \\ h & 0 & \epsilon_3 + V(x) \end{pmatrix} \begin{pmatrix} \psi_1(x) \\ \psi_2(x) \\ \psi_3(x) \end{pmatrix} dx = E \lim_{\epsilon \rightarrow 0} \int_{-\epsilon}^{\epsilon} \begin{pmatrix} \psi_1(x) \\ \psi_2(x) \\ \psi_3(x) \end{pmatrix} dx. \quad (19)$$

The operator function $\hat{g}(q)$ is defined by

$$\begin{aligned} \hat{g}(q) &= i \left(-te^{-ia\hat{q}/2} + t'e^{ia\hat{q}/2} \right) \\ &= i \sum_{n=0}^{\infty} \frac{a^n}{2^n n!} [t' - (-1)^n t] \frac{d^n}{dx^n} \end{aligned} \quad (20)$$

and

$$\hat{g}^*(q) = -i \sum_{n=0}^{\infty} \frac{a^n}{2^n n!} [-t + (-1)^n t'] \frac{d^n}{dx^n} \quad (21)$$

where the linear momentum is $\hat{q} = -i \frac{d}{dx}$. We performed the change $k = q + \pi/a_0$ for mirror symmetry bands respect to vertical axis, as shown in Fig. 2(b).

With the limit $\epsilon \rightarrow 0$ and considering the absence of singularities in $\psi_j(x)$ and $V(x)$, where $j = 1, 2$ and 3 , several integrals are equal to zero, but the equations with $\hat{g}(q)$ and $\hat{g}^*(q)$

$$\begin{aligned} \lim_{\epsilon \rightarrow 0} \int_{-\epsilon}^{\epsilon} \hat{g}(q) \psi_1(x) dx &= 0 \\ \lim_{\epsilon \rightarrow 0} \int_{-\epsilon}^{\epsilon} \hat{g}^*(q) \psi_2(x) dx &= 0 \end{aligned} \quad (22)$$

need and adequate treatment. Substituting the operator functions $\hat{g}(q)$ and $\hat{g}^*(q)$ in the integrals in Eq. (22), the matching conditions are given by

$$\begin{aligned} \hat{Q}(a) \psi_1(x) \Big|_{x=0^-} &= \hat{Q}(a) \psi_1(x) \Big|_{x=0^+} \\ \hat{Q}(-a) \psi_2(x) \Big|_{x=0^-} &= \hat{Q}(-a) \psi_2(x) \Big|_{x=0^+}, \end{aligned} \quad (23)$$

where the operator $\hat{Q}(a)$ is defined as

$$\hat{Q}(a) = \sum_{n=0}^{\infty} \frac{a^n}{2^n (n+1)!} [t' + (-1)^n t] \frac{d^n}{dx^n}. \quad (24)$$

The matching conditions, such as the Dirac Hamiltonian case, can be obtained by considering only the first term ($n = 0$) in the series (24).

The matching conditions (23) shall be imposed on the wave functions

$$\Psi_{\text{I}}(x) = \mathbf{u}(q_{\text{in}}) e^{iq_{\text{in}}x} + A_{\text{r}} \mathbf{u}(q_{\text{r}}) e^{iq_{\text{r}}x}, \quad (25)$$

in region I, and

$$\Psi_{\text{II}}(x) = A_{\text{t}} \mathbf{u}(q_{\text{t}}) e^{iq_{\text{t}}x} \quad (26)$$

as the transmitted wave function in region II. The calculations can be facilitated by these useful properties of $\hat{Q}(a)$

$$\begin{aligned} \hat{Q}(a) e^{i\lambda x} &= \sum_{n=0}^{\infty} \frac{(i\lambda a)^n}{2^n (n+1)!} [t' + (-1)^n t] e^{i\lambda x} \\ &= -2 \left[\frac{g(\lambda) + i(t-t')}{\lambda a} \right] e^{i\lambda x} \end{aligned} \quad (27)$$

and

$$\hat{Q}(-a) e^{i\lambda x} = -2 \left[\frac{g^*(\lambda) - i(t-t')}{\lambda a} \right] e^{i\lambda x}, \quad (28)$$

where $\lambda = q_{\text{in}/\text{r}/\text{t}}$. By using these relations for the wave functions (25) and (26), we have

$$\begin{aligned} [u_1(q_{\text{in}}) \hat{Q}(a) e^{iq_{\text{in}}x} + A_{\text{r}} u_1(q_{\text{r}}) \hat{Q}(a) e^{iq_{\text{r}}x}] \Big|_{x=0^-} &= \\ [A_{\text{t}} u_1(q_{\text{t}}) \hat{Q}(a) e^{iq_{\text{t}}x}] \Big|_{x=0^+} & \\ [u_2(q_{\text{in}}) \hat{Q}(-a) e^{iq_{\text{in}}x} + A_{\text{r}} u_2(q_{\text{r}}) \hat{Q}(-a) e^{iq_{\text{r}}x}] \Big|_{x=0^-} &= \\ [A_{\text{t}} u_2(q_{\text{t}}) \hat{Q}(-a) e^{iq_{\text{t}}x}] \Big|_{x=0^+}, \end{aligned} \quad (29)$$

which can be arranged in a matrix form as

$$\mathbf{w}(q_{\text{in}}) + A_{\text{r}} \mathbf{w}(q_{\text{r}}) = A_{\text{t}} \mathbf{w}(q_{\text{t}}). \quad (30)$$

The states $\mathbf{w}(q_{\text{in}/\text{r}/\text{t}})$ are defined by

$$\begin{aligned} \mathbf{w}(q_{\text{in}/\text{r}/\text{t}}) &= \\ (f(q_{\text{in}/\text{r}/\text{t}}) u^{(1)}(q_{\text{in}/\text{r}/\text{t}}), f^*(q_{\text{in}/\text{r}/\text{t}}) u^{(2)}(q_{\text{in}/\text{r}/\text{t}})), \end{aligned} \quad (31)$$

where the function $f(q_{\text{in}/r/t})$ is given by

$$f(q_{\text{in}/r/t}) = \frac{g(q_{\text{in}/r/t}) + i(t - t')}{q_{\text{in}/r/t}^a}. \quad (32)$$

In general, for a single interface Eq. (31) remains valid. Repeating the same procedure from Eq. (18) to Eq. (32) with a different Bloch Hamiltonian, the result can have a different form for the function $f(\mathbf{k})$. For two and three-dimensional lattices, the integration of Schrödinger equation in (18) is performed for the non-conserved component of the wave vector k_{\perp} , which is perpendicular to the interface. In the next sections, these general matching conditions for the wave functions will be applied to multiple systems that allow us to get unusual transport phenomena related to Klein tunneling effect.

FRESNEL-LIKE COEFFICIENTS: REFLECTION AND TRANSMISSION OF HEAVISIDE AND BARRIER POTENTIALS

In two- and three-dimensional ballistic systems, electron wave propagation can be described within an electron-optics framework, where electronic states behave as optical-like beams. Electrostatic gates in such junctions define effective refractive indices for electrons [3, 91, 111, 118–120], as illustrated by the typical electronic band structure shown in Fig. 3(a). The ballistic regime achieved in experimental settings can lead to negative refraction of electrons [117, 118]. When a linear interface separates two regions with different potentials, electrons tunnel by changing both group velocity and pseudo-spin and follow electron optical laws for the reflection and refraction phenomena, as well as the scattering probability [3, 31, 119]. The conservation of energy E , the component of wave vector k_y , and probability current density j_x helps to establish these electron optical laws, which are schematically represented using a kinematical construction, see Fig. 3(b).

In a junction, the electron scattering in the interface can be modeled by a step potential, as shown in Fig. 3(a). The regions I ($x < 0$) and II ($x \geq 0$) have the electrostatic potential 0 and V , respectively. The wave functions for both regions are written in terms of the eigenvectors of a general Bloch Hamiltonian as in Eqs. (25) and (26), where the quantities A_r and A_t are the wave amplitudes, while k_r and k_t are the wave vectors of the reflected and transmitted wave, respectively. The wave vectors \mathbf{k}_{in} , \mathbf{k}_r , and \mathbf{k}_t are evaluated in the eigenvector $\mathbf{u}(\mathbf{k}_{\text{in}/r/t})$ following the conservation of energy and linear momentum, as shown in Fig. 3(b) of the kinematical construction. Propagation modes occur if electrons with Fermi energy E from one of the bands cross to another band when there are allowed states. The direction of group velocity is given by the gradient of the energy band. With

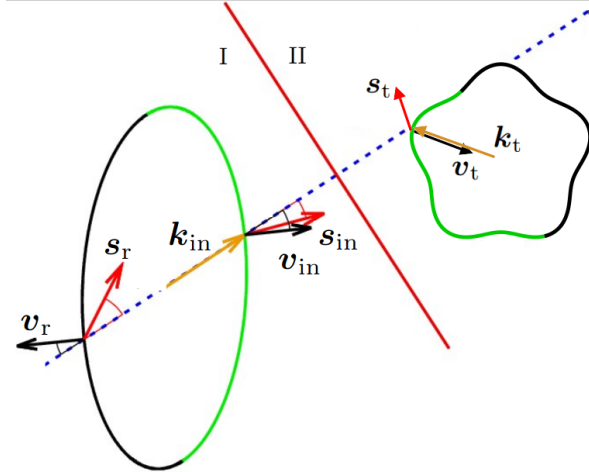
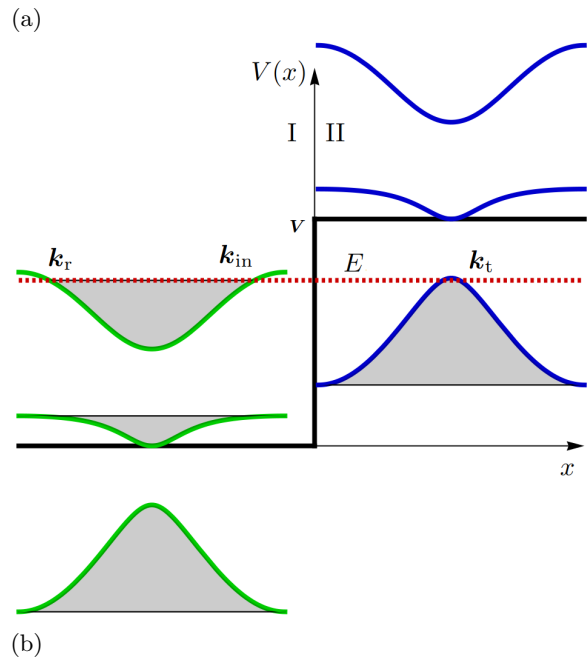


Figure 3. (a) Electronic band structure of a pn junction for an electrostatic step potential. The curves correspond the energy bands in regions I and II. The dashed red line indicates the Fermi level, where gray regions are the occupied states. (b) Kinematical construction represents the conservation of energy (energy contours), linear momentum (dashed line), and current density (green semi-arcs). The arrows indicate the direction of linear momentum $\mathbf{k}_{\text{in}/r/t}$, pseudo-spin $\mathbf{s}_{\text{in}/r/t}$, and group velocity $\mathbf{v}_{\text{in}/r/t}$ for the scattering of electrons at the interface (red line).

positive (negative) curvature, the group velocity points outwards (inwards) of the energy contour.

Returning to Eq. (30) and solving the 2×2 linear equation system, the reflection coefficient is

$$\begin{aligned}
R(\mathbf{k}_{\text{in}}) &= |A_r|^2 = \frac{|\mathbf{w}(\mathbf{k}_{\text{in}}) \times \mathbf{w}(\mathbf{k}_t)|^2}{|\mathbf{w}(\mathbf{k}_r) \times \mathbf{w}(\mathbf{k}_t)|^2} \\
&= \frac{|\mathbf{w}(\mathbf{k}_{\text{in}})|^2 \sin^2 \gamma(\mathbf{k}_{\text{in}}, \mathbf{k}_t)}{|\mathbf{w}(\mathbf{k}_r)|^2 \sin^2 \beta(\mathbf{k}_r, \mathbf{k}_t)}, \quad (33)
\end{aligned}$$

where \times indicates vectorial product of the states $\mathbf{w}(\mathbf{k}_{\text{in}})$ and $\mathbf{w}(\mathbf{k}_t)$. The relative pseudospin angle between the incident and transmitted states is defined by

$$\gamma(\mathbf{k}_{\text{in}}, \mathbf{k}_t) \equiv \arccos \left(\frac{|\mathbf{w}^*(\mathbf{k}_{\text{in}}) \cdot \mathbf{w}(\mathbf{k}_t)|}{|\mathbf{w}(\mathbf{k}_{\text{in}})| |\mathbf{w}(\mathbf{k}_t)|} \right). \quad (34)$$

For the reflected and transmitted states, the relative pseudospin angle is

$$\beta(\mathbf{k}_r, \mathbf{k}_t) \equiv \arccos \left(\frac{|\mathbf{w}^*(\mathbf{k}_r) \cdot \mathbf{w}(\mathbf{k}_t)|}{|\mathbf{w}(\mathbf{k}_{\text{in}})| |\mathbf{w}(\mathbf{k}_t)|} \right). \quad (35)$$

While that the transmission coefficient is given by

$$T(\mathbf{k}_{\text{in}}) = 1 - R(\mathbf{k}_{\text{in}}) \quad (36)$$

due to the current density conservation J_x . The reflection and transmission coefficients (33) and (36), respectively, can be related in terms of the hopping parameters and on-site energies of the tight-binding approach. To obtain exact or numerical wave vectors \mathbf{k}_{in} , \mathbf{k}_r , and \mathbf{k}_t involved in the scattering process, we use the complete energy bands of the Bloch Hamiltonian.

Let us examine the dynamics of quasi-particles in the presence of interfaces induced by localized fluctuations either in the hopping parameter or in the external electric field. We consider two distinct scenarios. In the first one, the interface arises from spatial inhomogeneity in the hopping parameter ω , which manifests itself as a rectangular barrier of the width D , as shown in Fig. 4

$$t_1 = \begin{cases} \tau_1, & x \in (-\infty, 0] \cup [D, \infty) \\ \tilde{\tau}_1, & x \in (0, D). \end{cases} \quad (37)$$

In the second one, a rectangular junction pnp with the following electric field will be considered.

$$V_{el} = \begin{cases} 0, & x \in (-\infty, 0] \cup [D, \infty) \\ V, & x \in (0, D). \end{cases} \quad (38)$$

The eigenvectors of the Bloch Hamiltonian $H(\mathbf{k})$ can be written in x -representation in the following form for each of the three regions,

$$\begin{aligned}
\Psi_{\text{I}}(\mathbf{r}) &= \mathbf{u}(\mathbf{k}_{\text{in}}) e^{i\mathbf{k}_{\text{in}} \cdot \mathbf{r}} + A_r \mathbf{u}(\mathbf{k}_r) e^{i\mathbf{k}_r \cdot \mathbf{r}} \\
\Psi_{\text{II}}(\mathbf{r}) &= A_a \mathbf{u}(\mathbf{k}_a) e^{i\mathbf{k}_a \cdot \mathbf{r}} + A_b \mathbf{u}(\mathbf{k}_b) e^{i\mathbf{k}_b \cdot \mathbf{r}} \\
\Psi_{\text{III}}(\mathbf{r}) &= A_t \mathbf{u}(\mathbf{k}_t) e^{i\mathbf{k}_t \cdot \mathbf{r}}, \quad (39)
\end{aligned}$$

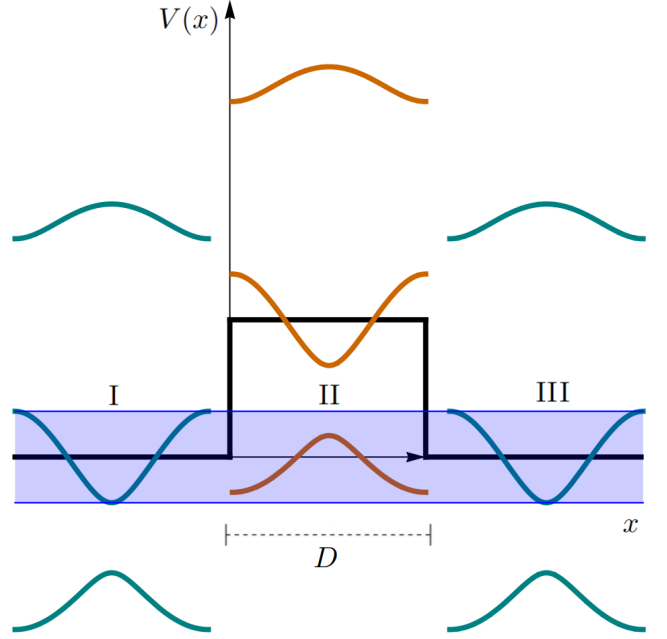


Figure 4. Electronic band structure of a bipolar nnp junction, which can be modeled through an electrostatic potential barrier. The curves correspond to energy bands; the blue area is the range of transmission from one of the conduction bands to the valence band.

The momenta \mathbf{k}_{in} and \mathbf{k}_r correspond to incident and reflected waves, respectively, while \mathbf{k}_a and \mathbf{k}_b are the wave vectors within the barrier. The explicit values of \mathbf{k}_a and \mathbf{k}_b depend on the nature of the barrier, i.e. they either depend on $\tilde{\tau}_1$ or on V , see (37) and (38).

With the two interfaces, in $x = 0$ and $x = D$, the reflection and transmission coefficients R and T are obtained by solving the following 4×4 linear equation systems, which are the result of applying the matching conditions (23)

$$\begin{aligned}
\mathbf{w}(\mathbf{k}_{\text{in}}) + A_r \mathbf{w}(\mathbf{k}_r) &= A_a \mathbf{w}(\mathbf{k}_a) + A_b \mathbf{w}(\mathbf{k}_b), \\
A_a e^{i\mathbf{k}_a D} \mathbf{w}(\mathbf{k}_a) + A_b e^{i\mathbf{k}_b D} \mathbf{w}(\mathbf{k}_b) &= A_t e^{i\mathbf{k}_t D} \mathbf{w}(\mathbf{k}_t). \quad (40)
\end{aligned}$$

Using the Cramer formula, the amplitude A_t is

$$A_t = \frac{\begin{vmatrix} |\mathbf{w}(\mathbf{k}_r) \mathbf{w}(\mathbf{k}_b)| & |\mathbf{w}(\mathbf{k}_{\text{in}}) \mathbf{w}(\mathbf{k}_b)| \\ |\mathbf{w}(\mathbf{k}_a) \mathbf{w}(\mathbf{k}_r)| & |\mathbf{w}(\mathbf{k}_a) \mathbf{w}(\mathbf{k}_{\text{in}})| \end{vmatrix}}{\begin{vmatrix} |\mathbf{w}(\mathbf{k}_r) \mathbf{w}(\mathbf{k}_b)| & |\mathbf{w}(\mathbf{k}_t) \mathbf{w}(\mathbf{k}_b)| e^{-i\mathbf{k}_a D} \\ |\mathbf{w}(\mathbf{k}_a) \mathbf{w}(\mathbf{k}_r)| & |\mathbf{w}(\mathbf{k}_a) \mathbf{w}(\mathbf{k}_t)| e^{-i\mathbf{k}_b D} \end{vmatrix}}, \quad (41)$$

where $|\mathbf{w}(\mathbf{k}_r) \mathbf{w}(\mathbf{k}_b)|$ is the determinant of the 2×2 matrix that has $\mathbf{w}(\mathbf{k}_r)$ and $\mathbf{w}(\mathbf{k}_b)$ as its columns. It is important to note that in Eq. (41), we have two nested determinants.

It is possible to get the simplest expression of Eq. (41), taking into account that $k_{x,r} = -k_{x,\text{in}}$ and $k_{x,a} =$

$-k_{x,b}$ for propagation modes. Therefore, the spinors are $\mathbf{w}(\mathbf{k}_r) = \mathbf{w}(\mathbf{k}_{in})^*$ and $\mathbf{w}(\mathbf{k}_b) = \mathbf{w}(\mathbf{k}_a)^*$. Defining $z_1 = |\mathbf{w}(\mathbf{k}_{in}) \mathbf{w}(\mathbf{k}_a)|$ and $z_2 = |\mathbf{w}(\mathbf{k}_{in}) \mathbf{w}(\mathbf{k}_a)^*|$, we have for the transmission

$$T = \frac{(|z_1|^2 - |z_2|^2)^2}{(|z_1|^2 - |z_2|^2)^2 \cos^2 k_a D + (|z_1|^2 + |z_2|^2)^2 \sin^2 k_a D}, \quad (42)$$

which is the generalization of the transmission found for chiral tunneling in graphene [4]. The Fabry-Pérot resonances are identical to the conventional one of constructive interference pattern of electromagnetic waves when $k_a D = n\pi$ with $n = 0, 1, 2, \dots$

GENERAL TRANSFER MATRIX METHOD APPLIED TO LOW-DIMENSIONAL LATTICES

To study the electron scattering of anisotropic materials considering stratified electrostatic potential media, as shown in Fig. 5, we consider adjacent potential barriers of width $x_n - x_{n-1}$ and height V_n , where n is the barrier index [89, 92, 113, 232–240]. The general matrix transfer method starts by writing the wave function ansatz for the barrier n as

$$\Psi^n(\mathbf{r}) = A_n \mathbf{u}(\mathbf{k}_n^a) e^{i\mathbf{k}_n^a \cdot \mathbf{r}} + B_n \mathbf{u}(\mathbf{k}_n^b) e^{i\mathbf{k}_n^b \cdot \mathbf{r}}, \quad (43)$$

where A_n and B_n are the amplitudes of the wave inside the barrier. For the first region, $n = 0$, the incident wave has an amplitude $A_0 = 1$ and wave vector $\mathbf{k}_0^a = \mathbf{k}_{in}$, for the reflected part, the amplitude is $B_0 = A_r$ and wave vector $\mathbf{k}_0^b = \mathbf{k}_r$. With $n = N + 1$ in the last region, $B_{N+1} = 0$ because there is no reflection, and the transmitted amplitude is $A_{N+1} = A_t$.

Applying the matching conditions of Eq. (23) at $x = x_n$ that separates the regions with wave functions $\Psi^n(\mathbf{r})$ and $\Psi^{n+1}(\mathbf{r})$, we have

$$\begin{pmatrix} A_{n+1} \\ B_{n+1} \end{pmatrix} = M_{n+1n}^{-1} M_{nn} \begin{pmatrix} A_n \\ B_n \end{pmatrix}, \quad (44)$$

where the matrices M_{ml} are

$$M_{ml} = \begin{bmatrix} \mathbf{w}(\mathbf{k}_n^a) & \mathbf{w}(\mathbf{k}_n^b) \end{bmatrix} \begin{pmatrix} e^{ik_{x,n}^a x_l} & 0 \\ 0 & e^{ik_{x,n}^b x_l} \end{pmatrix}, \quad (45)$$

which taken into account the conservation of k_y parallel to the interfaces at $x = x_n$ and the substitution $\mathbf{u}(\mathbf{k}_n) \rightarrow \mathbf{w}(\mathbf{k}_n)$ given by Eq. (31). It is possible to get a 2×2 linear equation system involving only A_r and A_t for the first and last regions by defining the matrix of the stratified potential media

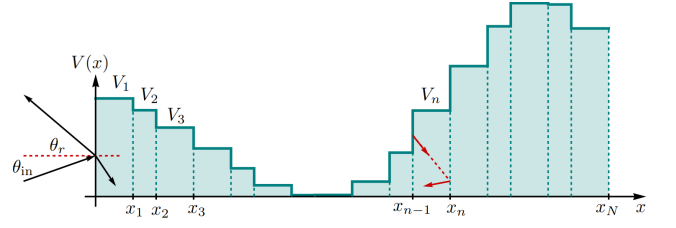


Figure 5. Arbitrary electrostatic potential modeled as a series of potential barriers, where the transfer matrix method can be used.

$$\Lambda \equiv \prod_{n=1}^N \mathcal{M}_n \Theta_n \mathcal{M}_n^{-1}, \quad (46)$$

where the multiplication is performed from left to right, increasing the index n . The matrix \mathcal{M}_n is

$$\mathcal{M}_n = \begin{bmatrix} \mathbf{w}(\mathbf{k}_n^a) & \mathbf{w}(\mathbf{k}_n^b) \end{bmatrix} \quad (47)$$

and

$$\Theta_n = \begin{pmatrix} e^{-ik_{x,n}^a(x_n - x_{n-1})} & 0 \\ 0 & e^{-ik_{x,n}^b(x_n - x_{n-1})} \end{pmatrix}. \quad (48)$$

The matrix Λ contains all the information about the electron crossing a stratified electrostatic potential medium. The effect of Λ is similar to replacing the stratified media by a single interface at $x = 0$, and therefore, the transmission is identical to pn junctions, as discussed in the previous section. The equation of a pn junction-like is

$$\mathbf{w}(\mathbf{k}_{in}) + A_r \mathbf{w}(\mathbf{k}_r) = A_t e^{ik_{x,t} x_{N+1}} \Lambda \mathbf{w}(\mathbf{k}_t), \quad (49)$$

which is identical to Eq. (30). Hence, the reflection coefficient is similar to Eq. (33)

$$R(\mathbf{k}_{in}) = |A_r|^2 = \frac{|\mathbf{w}(\mathbf{k}_{in}) \times \Lambda \mathbf{w}(\mathbf{k}_t)|^2}{|\mathbf{w}(\mathbf{k}_r) \times \Lambda \mathbf{w}(\mathbf{k}_t)|^2}. \quad (50)$$

It is worth mentioning that this transfer method embodies known results for pn junctions of graphene, transistors, and one-dimensional superlattices [3, 4, 153]. From Eq. (50), it is clear that the perfect transmission is reached when the effective incident one-half pseudospin $\mathbf{w}(\mathbf{k}_{in})$ is parallel to the transmitted pseudospin $\Lambda \mathbf{w}(\mathbf{k}_t)$, while total reflection appears if $|\mathbf{w}(\mathbf{k}_{in}) \times \Lambda \mathbf{w}(\mathbf{k}_t)| = |\mathbf{w}(\mathbf{k}_r) \times \Lambda \mathbf{w}(\mathbf{k}_t)|$. Therefore, the relative angle of the states $\mathbf{w}(\mathbf{k}_{in})$ and $\Lambda \mathbf{w}(\mathbf{k}_t)$ can indicate the emergence of Klein and anti-Klein tunneling as

$$\gamma(\mathbf{k}_{in}, \mathbf{k}_t) = \arccos \left(\frac{|\mathbf{w}^*(\mathbf{k}_{in}) \cdot \Lambda \mathbf{w}(\mathbf{k}_t)|}{|\mathbf{w}(\mathbf{k}_{in})| |\Lambda \mathbf{w}(\mathbf{k}_t)|} \right), \quad (51)$$

where $\gamma(\mathbf{k}_{in}, \mathbf{k}_t) = 0$ and $\gamma(\mathbf{k}_{in}, \mathbf{k}_t) = \pi/2$ correspond to Klein and anti-Klein tunneling, respectively.

THE EMERGENCE OF KLEIN AND ANTI-KLEIN TUNNELING

The absence of backscattering on electric barriers in normal direction was understood as a consequence of topological singularity identified with a Dirac point, see [241], [242], or as a result of the pseudospin conservation [4]. A key point in the absence of back-scattering is the conservation of pseudo-spin, that explains the perfect transmission of massless Dirac fermions in potential barriers [3]. The Heisenberg picture indicates that the conservation of pseudo-spin along the direction x is given by

$$\frac{d\sigma_x}{dt} = \frac{i}{\hbar} [\hat{H}, \sigma_x]. \quad (52)$$

The Hamiltonian must depend straightforwardly on σ_x , and therefore, the pseudo-spin $s_x = \hbar\sigma_x/2$ is a constant of motion. This fact occurs under normal incidence of electrons in an electrostatic potential in graphene, where the Hamiltonian is written as $H = v_F\sigma_x p_x + V(x)$, being v_F the Fermi velocity, p_x the linear momentum, and $V(x)$ the electrostatic potential [4].

The absence of backscattering can be also explained by a unitary transformation that maps the subsystem with perfect transmission into the free-particle dynamics [243]. Indeed, let us consider the two-dimensional Dirac fermion in presence of an electric barrier that has translational symmetry described effectively by a two-dimensional Dirac equation. The fermions bouncing on the barrier in normal direction ($k_y = 0$) are governed by the following operator

$$H_{k_y=0} = e^{-ik_y y} (-i\sigma_x \partial_x - i\sigma_y \partial_y + V(x)) e^{ik_y y} |_{k_y=0}. \quad (53)$$

The operator can be mapped to the free-particle Hamiltonian via the unitary transformation

$$U = e^{i\alpha\sigma_x} = \cos \alpha + i \sin \alpha \sigma_x, \quad U^\dagger = U^{-1}, \quad (54)$$

dependent on the interaction potential,

$$\alpha(x) = \frac{1}{v_F} \int^x V(\tau) d\tau. \quad (55)$$

Indeed, there holds

$$U H_{k_y=0} U^{-1} = -i\sigma_1 \partial_x - i\sigma_2 \partial_y. \quad (56)$$

The relation justifies the absence of reflection in the system governed by $H_{k_y=0}$ as there are no back-scattered waves in the free-particle system. The unitary mapping can be also used for deformation of both the vector potential and effective mass [244].

However, related phenomena, such as super-Klein tunneling of massive pseudo-spin-one particles, do not seem to follow from the pseudo-spin conservation. The spin-orbit Hamiltonian for super-Klein tunneling is $H = v_F \mathbf{S} \cdot \mathbf{p} + U$, where U is the mass term and \mathbf{S} is a spin-one operator [19]. If we apply again the Heisenberg picture, the omnidirectional perfect transmission involves both components in the linear momentum \mathbf{p} , then

$$\frac{d\mathbf{S}}{dt} = \frac{i}{\hbar} [\hat{H}, \mathbf{S}] \neq 0, \quad (57)$$

which leads to the non-conservation for the pseudo-spin one operator. The usual explanation for super-Klein tunneling is due to the special matching condition of the wave function at the interface. In the present, we established a general condition that embodies the emergence of Klein tunneling in graphene, super-Klein tunneling in pseudo-spin one systems, and anti-Klein tunneling of bilayer graphene and phosphorene, through the definition of a shortened pseudo-spin 1/2 from the wavefunction continuity. The shortened spinor appears when the boundary conditions are applied at the interface for the eigenvectors of the Bloch Hamiltonian, as seen in Eq. (31). The perfect transmission (reflection) occurs when the incident spinor \mathbf{w}_i is parallel (perpendicular) to the transmitted state $\Lambda \mathbf{w}_t$, giving rise to the Klein (anti-Klein) tunneling, as seen in Eqs. (33) and (50).

TYPES OF KLEIN TUNNELING BEYOND GRAPHENE: ANOMALOUS, ANTI-KLEIN, AND SUPER-KLEIN TUNNELING

The previous sections established the methodologies for exploring the transmission of waves in synthesized and artificial crystals under position-dependent potentials. In the following subsections, we present several types of Klein and anti-Klein tunneling in low-dimensional systems for massless and massive particles.

Klein tunneling in one-dimensional chains

To study particle transmission in one-dimensional chains, such as Su-Schrieffer-Heeger (SSH) lattices in pnj junctions, we analyze the transmission as a function of the energy E and electrostatic potential of the barrier V , as shown in Fig. 6(a)-(c). To identify possible signatures of Klein tunneling, we focus on areas of high transmission. It is well known that the SSH lattices undergo a topological phase transition upon tuning one of the hopping parameters: the system is in a trivial (topological) phase for $t < t'$ ($t > t'$) [105, 171, 181, 215, 229, 245–254], where the winding number is the topological invariant that characterizes these phases, see Fig. 6(d)-(f).

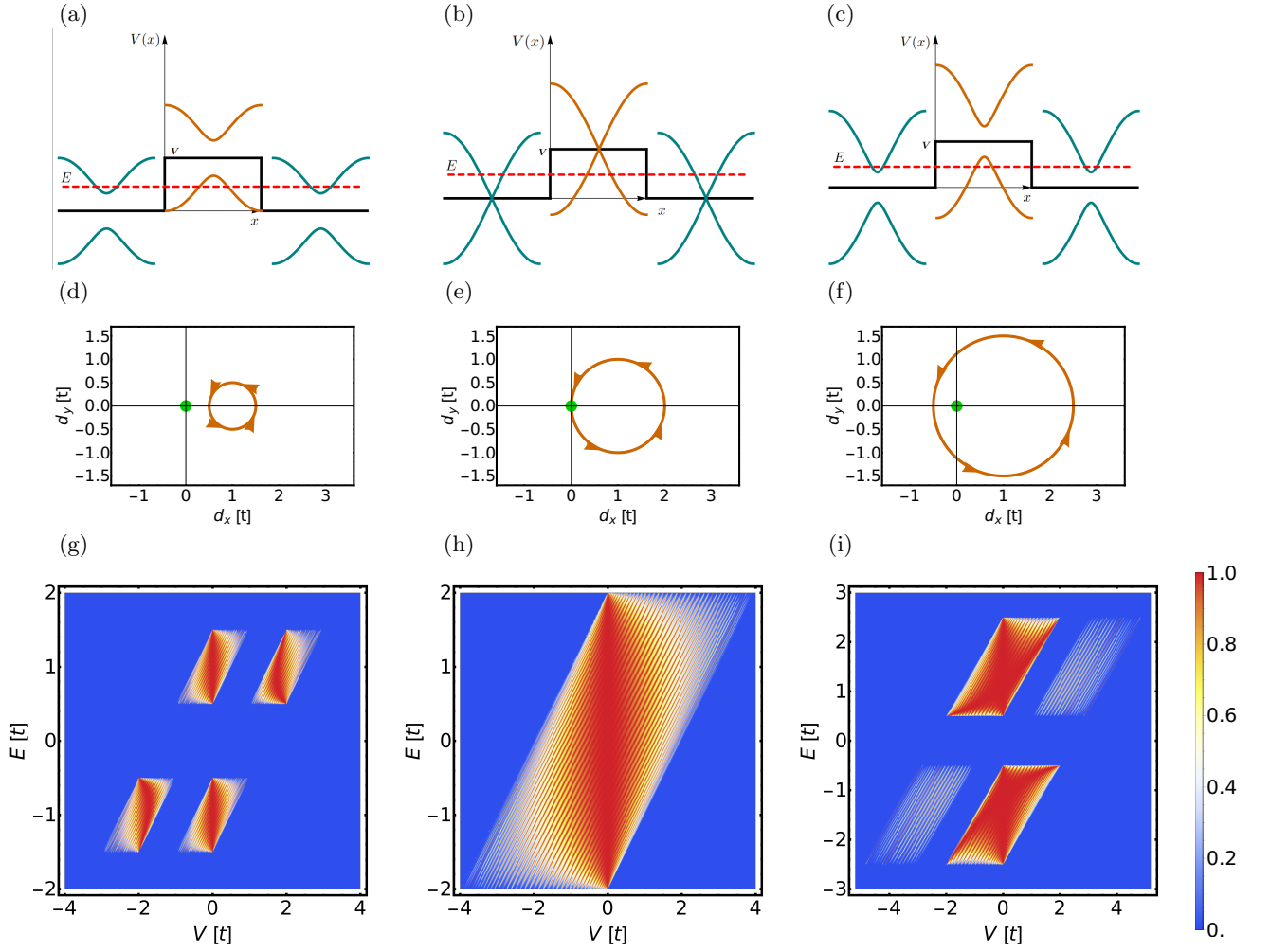


Figure 6. Electronic band structure of a bipolar junction based on Su-Schrieffer-Heeger chain. The curves indicates the energy bands for the trivial (a), critical (b), and topological phase (c). The dashed red line is the Fermi level E and V the barrier height, which can be negative for well potentials. Pseudo-spin loops in the Bloch plane for the trivial (d), critical (e), and topological phase (f). The green circle pointed out the origin of Bloch plane. Electron transmission as a function of the Fermi level E and barrier height V . (g) Trivial phase has the set of values $t = 1$ and $t' = 0.5$, (h) the parameters for the critical topological phase transition are $t = t' = 1$, and (c) topological phase with $t = 1$ and $t' = 1.5$. The barrier width is $D = 25$ in units of a .

This transition strongly influences both interband and intraband tunneling in the whole regimens of the bipolar junction from $nn'n$ to $pp'p$, as shown in Fig. 6. We compute the transmission in the trivial ($t < t'$), critical ($t = t'$), and topological ($t > t'$) phase using Eq. (42), taking into account that the SSH chain is described by the Bloch Hamiltonian

$$H_{SSH}(k) = \begin{pmatrix} 0 & t - t'e^{-ik} \\ t - t'e^{ik} & 0 \end{pmatrix}, \quad (58)$$

which warranties the simple relation of wave numbers $k_{in} = -k_r$. The length of the unit cell is $a_c = 1$. The matching conditions for the wave function with the Hamiltonian in Eq. (58) gives rise to the effective pseudo-spin vectors in Eq. (23), where the functions $f(k)$ are

$$f(k_{in/r/t/a/b}) = \frac{e^{ik_{in/r/t/a/b}} - 1}{k_{in/r/t/a/b}}. \quad (59)$$

The conservation energy E allows us to relate $k_{in/r/t/a/b}$ in terms of E , the barrier height V , and hopping parameters

$$\begin{aligned}
k_{\text{in}}(E) &= -k_r(E) = k_t(E) \\
&= \text{sgn}(E) \arccos\left(\frac{t^2 + t'^2 - E^2}{2tt'}\right) \\
k_a(E, V) &= -k_b(E, V) \\
&= \text{sgn}(E - V) \arccos\left(\frac{t^2 + t'^2 - (E - V)^2}{2tt'}\right).
\end{aligned} \tag{60}$$

With these relations in Eq. (60), the transmission coefficient in Eq. (42) can be expressed as a function of E and V . The transmission features, as shown in Fig. 6, are explained by using the relative pseudospin direction, which is given by Eq. (51). Although the SSH chain is one-dimensional, the orientation of the pseudospin is represented by the polar angles α and ϕ in the Bloch sphere. The electron scattering involves reduced components of the spinors as indicated in Eq. (40), we can relate these spinors in the Bloch sphere for the incident, reflected, and transmitted states with the set of angles $(\alpha_{\text{in}}, \phi_{\text{in}})$, (α_r, ϕ_r) , and (α_t, ϕ_t) as a function of k_{in} . Nevertheless, our interest is to get the relative angle $\gamma(k_{\text{in}}, k_t)$ between the incident and transmitted state in Eq. (51), since that reflection and transmission depend on this angle. In the case of evanescent waves, total internal reflection is obtained. In such a situation, the definition of $\gamma(k_{\text{in}}, k_t)$ in Eq. (51) has a real value. However, to indicate this total reflection we can define the constant value of $\gamma = \pi/2$. For propagation states, the value of $\gamma = \pi/2$ in Eq. (34) is not excluded. If the pseudospin of incident and transmitted states is perpendicular, an anti-Klein tunneling appears [4, 114]. One simple explanation of the perfect transmission that gives rise to Klein tunneling is the conservation of the pseudo-spin \mathbf{w} . The relative difference in the pseudospin angle in Eq. (51) indicates that perfect tunneling emerges when $\gamma = 0$, such as Klein tunneling in graphene [4].

In Fig. 6(g), Klein tunneling appears for the negative $nn'n$ and positive $pp'p$ regimen. The reddish region for the vertical line in $V = 0$ is the absence of scattering, while bluish regions emerge due to evanescent waves in the scattering process. The different regimes for interband (npn and pnp) and intraband tunneling ($nn'n$ and $pp'p$) are separated by the energy band gap of the SSH chain in the trivial phase $2\Delta = 2|t - t'|$. Since the transmitted wave vector k_a and k_t have imaginary part, the relative pseudospin angle is $\gamma = 90^\circ$ and the transmission is zero by total internal reflection. The interference patterns within the regimens are due to the Fabry-Pérot resonances $k_a D = n\pi$, where D is the barrier width.

The hopping parameter t' controls the topological phase transition in the SSH chain and Klein tunneling for intraband tunneling disappear in the critical value $t = t'$, [see Fig. 6(h)]. Due to the closing in the band

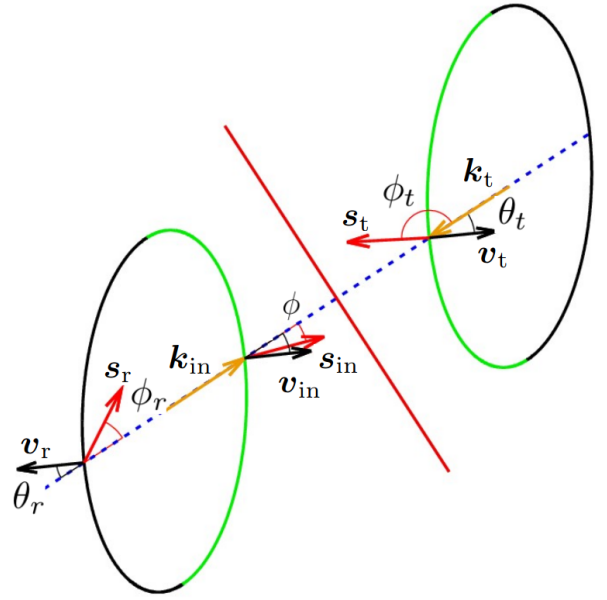


Figure 7. Kinematical construction for the focusing condition, when $V = 2E$, which represents the conservation of energy (energy contours), linear momentum (dashed blue line), and current density (green semi-arcs). The arrows indicate the direction of linear momentum $\mathbf{k}_{\text{in}/r/t}$, pseudo-spin $\mathbf{s}_{\text{in}/r/t}$, and group velocity $\mathbf{v}_{\text{in}/r/t}$ for the scattering of electrons at the interface (red line).

gap, the four regions for the transmission merge. In contrast, passing from the trivial to the topological phase, the Klein tunneling changes its location now in the interband tunneling regimens, as seen in Fig. 6(i). The four regimens npn , $nn'n$, pnp , and $pp'p$ are again separated in the topological phase by the opening in the gap. The most remarkable feature is that the topological phase transition interchanges the Klein tunneling from intraband to interband tunneling.

Anomalous Klein tunneling in anisotropic two-dimensional materials

Anomalous Klein tunneling refers to perfect transmission occurring away from normal incidence, enabled by the conservation of pseudospin. This effect arises in anisotropic 2D materials, such as borophene and strained graphene [31, 219, 236, 255–257]. In this section, we analyze anomalous Klein tunneling in a general anisotropic hexagonal lattice subjected to an electrostatic and stratified potential. The study is addressed within a low-energy regimen using the matrix transfer formalism.

The Bloch Hamiltonian in Eq. (14) is simplified by expanding up to first order in \mathbf{k} around the Dirac point. We found the following Dirac-type Hamiltonian that de-

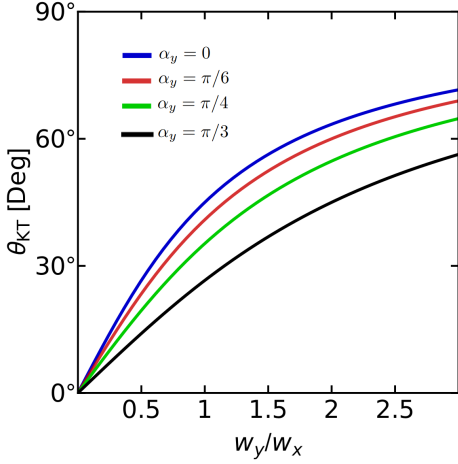


Figure 8. Anomalous Klein tunneling angle of Eq. (67) as a function of w_y/w_x ratio with the set of values for the velocity phases $\alpha_x = 0$ and $\alpha_y = 0, \pi/6, \pi/4$ and $\pi/3$.

scribes spin-1/2 quasi-particles,

$$H = \begin{pmatrix} 0 & \omega^* \cdot \mathbf{p} \\ \omega \cdot \mathbf{p} & 0 \end{pmatrix} + V \quad (61)$$

where $\mathbf{p} = (p_x, p_y)$ is the linear momentum, $\omega = (w_x e^{i\alpha_x}, w_y e^{-i\alpha_y})$ is the complex velocity, and V is the constant potential. We note that the operator acquires the Dirac-type standard form for the values $\alpha_x = 0$ and $\alpha_y = -\pi/2$.

The dispersion relation for the simplified Hamiltonian in Eq. (61) reads as follows

$$|E - V| = \sqrt{w_x^2 p_x^2 + w_y^2 p_y^2 + 2w_x w_y p_x p_y \cos(\alpha_x + \alpha_y)}, \quad (62)$$

where the components p_x and p_y of linear momentum are parametrized as

$$\begin{aligned} p_x &= \pm s(w_y/w_x)\rho \sin(\alpha_x + \alpha_y \mp \chi) \\ p_y &= \rho \sin \chi. \end{aligned} \quad (63)$$

The minus in p_x indicates the reflection for region I. The angle χ is a useful parameter that allows us to obtain simple expressions for reflection and Snell's law. The quantity $s = \pm 1$ is the band index. Starting from elliptical energy contours in Eq. (62), which are typical of anisotropic materials such as strained graphene, phosphorene, and borophene, the refraction index ρ is shown to be the half-width of the ellipse (see Fig. 7)

$$\rho_j = |E - \delta_{2j}V|/[w_y \sin(\alpha_x + \alpha_y)], \quad (64)$$

where the Kronecker delta switches the potential value with $j = 1$ and 2 for regions I and II, respectively. The

definition of pseudo-spin angle and conservation of p_y allow us to derive the analogue of Snell's law for the interface created by the electric barrier. Indeed, the conservation of p_y is given by $\rho_1 \sin \chi_{\text{in}} = \rho_2 \sin \chi_t$, where χ_{in} and χ_t are angles related to the incidence and refraction angles θ_{in} and θ_t from the group velocity, respectively. In general, for an anisotropic dispersion relation, reflected electron beams do not follow the typical reflection law $\theta_{\text{in}} = \theta_r$, due to the rotation of the elliptical Dirac cone.

To obtain the appropriate direction of the electron beam, we calculate the group velocity $\mathbf{v} = (v_x, v_y)$, which is given by

$$\begin{aligned} v_x &= \partial_{p_x} E = \frac{w_x^2 p_x + w_x w_y p_y \cos(\alpha_x + \alpha_y)}{E}, \\ v_y &= \partial_{p_y} E = \frac{w_y^2 p_y + w_x w_y p_x \cos(\alpha_x + \alpha_y)}{E}. \end{aligned} \quad (65)$$

The direction of the group velocity is then specified by $\tan \theta = \frac{v_y}{v_x}$ and indicates the electron beam direction. It can be expressed in terms of χ

$$\tan \theta = \pm \frac{w_y \cos[\chi \mp s(\alpha_x + \alpha_y)]}{w_x \cos \chi}. \quad (66)$$

The sign minus corresponds to the reflection angle θ_r . The substitutions $\theta \rightarrow \theta_t$, $\chi \rightarrow \chi_t$, and $s \rightarrow s'$ allow us to obtain the relation of the refraction angle θ_t and χ_t with the sign plus in Eq. (66). Since $\chi = \chi_t = 0$ leads to the conservation of pseudo-spin, the angular shift of the anomalous KT is

$$\theta_{\text{KT}} = \arctan \left[\frac{w_y}{w_x} \cos(\alpha_x + \alpha_y) \right]. \quad (67)$$

This result is independent of the Fermi level and potential profile. The angle for the KT can be tuned by the anisotropic parameters of the velocity w_x and w_y . This special angle allows us to write the reflection and Snell's law in a straightforward way

$$\tan \theta_r = \tan \theta_{\text{in}} - 2 \tan \theta_{\text{KT}} \quad (68)$$

$$\tan \theta_t = s s' \tan \theta_{\text{in}} + (1 - s s') \tan \theta_{\text{KT}}, \quad (69)$$

where the last expression corresponds to the special case of Snell's law when the focusing condition $\rho_1 = \rho_2$ is satisfied for elliptical energy contours with the same vertical half-width, as shown in Fig. 7. These optical laws embody unusual effects such as negative reflection and refraction of electrons impinging on the interface [31, 111, 117, 258]. Since the elliptical Dirac cone is rotated on both sides of the junction, the outgoing electron beam has a v_y component different from zero.

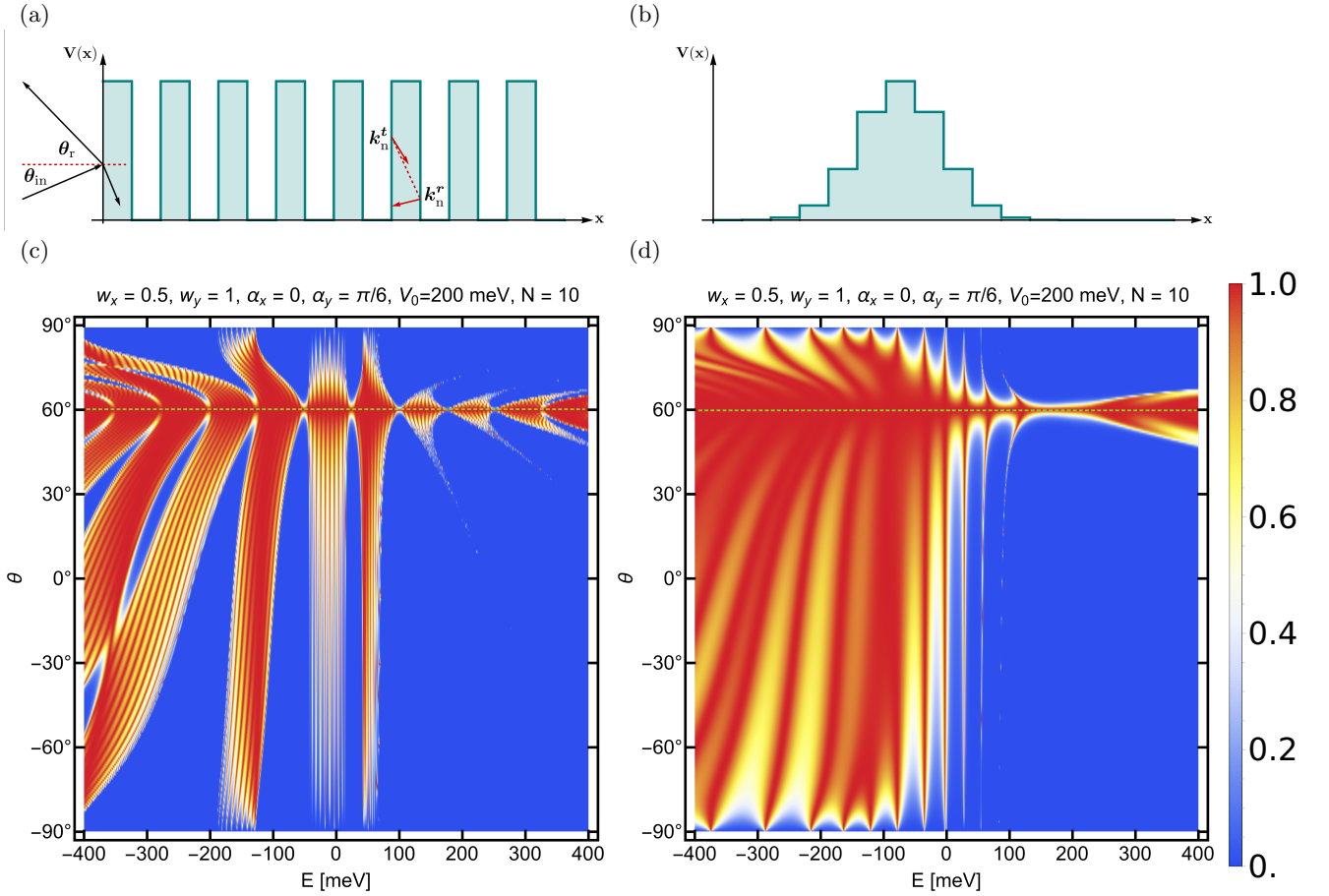


Figure 9. Electron transmission for electrostatic potentials as a function of energy and incidence angle. (a) and (b) Periodic and Gaussian-like profile as a set of potential barriers. (c) and (d) Transmission coefficient corresponding to the stratified potential profile in (a) and (b), respectively. The anomalous Klein tunneling in $\theta = 60^\circ$ (green dashed line) is independent of the shape of electrostatic potential, but the Fabry-Pérot resonances present drastic changes due to the electrostatic potential profile.

In contrast, Klein tunneling in graphene occurs only for normal incidence [4]. In anisotropic materials with rotated elliptical Dirac cones, however, the angle for Klein tunneling can be modulated through the complex velocities ω . In Fig. 8, the Klein tunneling angle depends on the velocity phases $\alpha_{x,y}$ and on the ratio w_y/w_x . Importantly, this perfect transmission is not resonant and independent of the electrostatic potential, as a direct consequence of the conservation of the pseudo-spin. This phenomenon, known as anomalous Klein tunneling, can be controlled via strain [31, 219, 236].

The anomalous Klein tunneling persists from a single interface of a *pn* junction or through stratified potential media. For instance, using a periodic electrostatic potential in Fig. 9(a), we show the transmission as a function of incidence angle θ_{in} and Fermi level energy E in Fig. 9(c). The anomalous Klein tunneling appears in positive incidence, for the particular case treated here, $\alpha_x = 0$, $\alpha_y = \pi/6$, $w_x = 0.5$, and $w_y = 1$, giving rise to a deviation of $\theta_{\text{KT}} = 60^\circ$ from Eq. (67). Nevertheless,

for negative angles, the other set of resonances remains almost constant. This is due to the anisotropy of the dispersion relation.

To show that the anomalous Klein tunneling is independent of the electrostatic potential, we change the periodic potential barrier by a set of subsequent barriers that follows a gaussian profile, see Fig. 9(b) and (d). We can observe how the perfect transmission remains in the angle $\theta_{\text{KT}} = 60^\circ$, as previous periodic case. Moreover, the resonances are closer for positive incidence angles. Contrary to the case of negative angles, where resonances are separated from each other. If we change the velocity phase α_y to negative values, the anomalous Klein tunneling appears at negative incidence angles. The transmission can be valley-independent because the values of w_x , w_y , α_x , and α_y are considered the same for the whole material. The valley-dependence can appear in borophene and graphene when the system has inhomogeneity regions of hopping parameters [142].

When the electrostatic potential is periodic, as shown

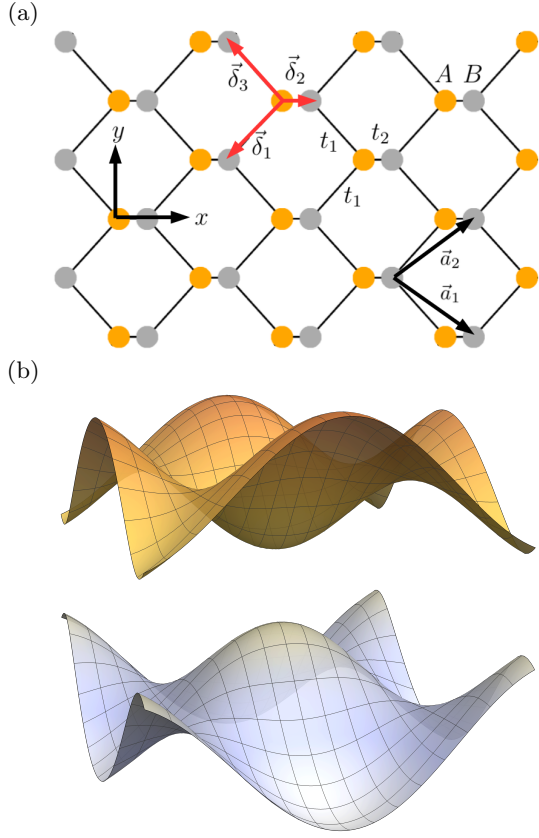


Figure 10. (a) Top view of the lattice structure of phosphorene, where two non-equivalent sites are considered in the tight-binding approach. (b) The electronic band structure shows a band gap and a strong anisotropic dispersion relation.

in Fig. 9(a) and (c), the transmission has alternating zones of minimum and maximum values as a function of the Fermi level. It takes higher values for larger incidence angles when $E < V$ due to the Fabry-Pérot interference. The resonances become more defined in the range of $E > V$, and their width becomes narrower. While $E < V$, a wide range of incidence angle values shows maximum transmission. Energy minigaps ($T = 0$) emerge for electrons under oblique incidences due to destructive interferences. These minigaps follow a fractal structure if the number of barriers is increased. In contrast with Gaussian potential profiles, where energy minigaps are less, see Fig. 9(d).

Anti-Klein tunneling in two-dimensional materials

Anti-Klein tunneling is a total reflection by the pseudo-spin momentum locking. When compared to the total internal reflection, which is due to evanescent waves, anti-Klein tunneling possesses allowed energy states. How-

ever, these states are not accessible because the effective pseudo-spin for incident waves is perpendicular to transmitted one states [4, 111–114, 259–263]. One way to observe anti-Klein tunneling is under normal incidence of electrons in a pn junction of bilayer graphene [4]. Herein, we studied the anti-Klein and anti-super-Klein tunneling of phosphorene under the special condition $V = 2E$, where electrons go from the conduction band in region I to the valence band in region II. The lattice and band structure of phosphorene are shown in Fig. 10. By expanding the tight-binding Hamiltonian in Eq. (14) around the Γ point in the center of the first Brillouin zone [111, 225, 226], we have

$$H_{\text{ph}}(\mathbf{k}) = \left(\Delta^2 + \frac{k_x^2}{2m_x} + \frac{k_y^2}{2m_y} \right) \sigma_x + vk_x \sigma_y, \quad (70)$$

which has an anisotropic dispersion relation, as shown in Fig. 10(b), where Δ is the semigap, m_x and m_y are the anisotropic masses, and v is the velocity limit of pseudo-relativistic particles. These effective quantities are related to the hopping parameters t_1 and t_2 [111, 119, 209, 224, 259].

Due to the anisotropy in the dispersion relation, the reflection angle θ_r as a function of the incidence angle θ_{in} does not satisfy the conventional reflection law, since the tilted pn junction of phosphorene in Fig. 11(a) can have negative reflection [111]. The angle α controls the tilt of the junction. The typical reflection law $\theta_r = \theta_{\text{in}}$ is found only for junctions parallel to the x ($\alpha = 0^\circ$) and y axes ($\alpha = \pm 90^\circ$), but in general θ_r is a non-linear function of θ_{in} . Following an identical procedure for the reflection law in Eq. (68), the reflection law is [111]

$$\tan \theta_r = \tan \theta_{\text{in}} - 2 \tan \theta_B, \quad (71)$$

where the backscattered angle θ_B , which corresponds to the case $\theta_r = -\theta_{\text{in}}$, is defined by

$$\tan \theta_B = \frac{(1 - \lambda) \tan \alpha}{(1 + \lambda) \tan \alpha}, \quad (72)$$

being $\lambda = (m_y/m_x)(1 + m_x v^2/\Delta)$, a term that depends on the effective parameters of the phosphorene Hamiltonian, as seen in Eq. (70). This negative reflection appears for certain values of the tilt angle α in the incidence range $0 < |\theta_{\text{in}}| < |\theta_M|$, where θ_M is the incidence angle for normal reflection. For $|\theta_i| > |\theta_M|$, anomalous reflection is observed, because θ_{in} and θ_r have the same sign but different values. Moreover, backscattering $\theta_r = -\theta_{\text{in}}$ emerges for certain incidence angles. The breaking of the reflection law in pn junctions of phosphorene is independent of V , and therefore, it is valid for when $V \neq 2E$.

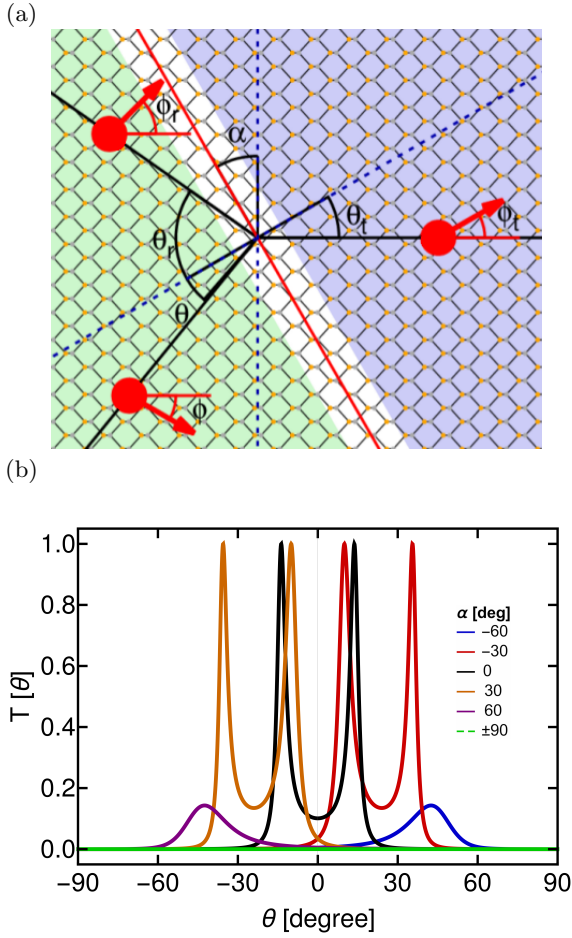


Figure 11. (a) Electron scattering of a tilted phosphorene pn junction with the schematic representation of the group velocity and pseudo-spin direction. (b) Transmission as a function of incidence angle of electrons impinging a potential barrier V for different tilted angles α .

Negative reflection can be viewed from the kinematical construction in Fig. 7, the conserved linear momentum parallel to the interface, which is represented by the dashed line, intersects the points for the conserved energy contours. The component of group velocity parallel to the interface becomes different for incident, reflected, and transmitted waves. Only if $\alpha = 0^\circ, \pm 90^\circ$, these states have the conserved group velocity by causing the conventional reflection $\theta_{\text{in}} = \theta_r$. It is worth noticing that atypical reflection is explained by the fact that the tilting of the junction breaks the mirror symmetry with respect to the k_x and k_y axes in momentum space.

We consider a bipolar junction based on phosphorene, where the transmission as a function of incidence angle θ_{in} is shown in Fig. 11(b) and it is calculated using Eq. (42). By changing the tilting of the junction α , the non-resonant transmission is always less than one to difference of Klein tunneling, which is observed in graphene [4, 7]. Remarkably, zero transmission is observed for the

angle $\alpha = \pm 90^\circ$ in the whole incidence angles. This omni-directional total reflection, called anti-super Klein tunneling, occurs when the effective states $\mathbf{w}(\mathbf{k}_{\text{in}})$ and $\mathbf{w}(\mathbf{k}_t)$ are perpendicular, as indicated in Eq. (51). In contrast to total internal reflection, it is not caused by the evanescent modes due to the band gap, since there exist states allowed energetically [111, 119, 259]. The perfect transmission observed in Fig. 11(b) is due to Fabry-Pérot resonances with a tilted angle $\alpha \neq 90^\circ$. The anisotropy of phosphorene and other materials, such as strained graphene [31] and black phosphorus [259], is responsible of anisotropic transport [88, 166, 256, 264], negative reflection [111], perfect waveguides [112], electronic cloaking [113, 260, 265], asymmetric Veselago lenses, super-Klein tunneling modulated by linearly polarized light [42], and Goos-Hänchen effect [109].

Super-Klein tunneling of pseudo-spin one systems

For crystals with three atoms in the unit cell, it is possible, in some particular cases, to relate the Bloch Hamiltonian in terms of spin-one matrices. Two outstanding examples are the dice and Lieb lattices [10, 11, 27, 41, 47, 49, 50, 52, 56, 86, 103, 146–148, 228, 266–274]. In such lattices, super-Klein tunneling can emerge for both massless and massive particles in the focusing condition $V = 2E$ of Veselago lenses. In the continuum approximation, the Bloch Hamiltonian of the dice or Lieb lattice can be approximated to a spin-one Hamiltonian around a high symmetry point as

$$H_1 = \hbar v_F \mathbf{S} \cdot \mathbf{k} + \Delta U, \quad (73)$$

where $\mathbf{S} = (S_x, S_y)$ are the spin-one matrices and $U = S_z$ or M as a matrix representing the mass term [19], which is responsible for the gap opening. The dispersion relation of the electron under the Hamiltonian H_1 is $E_\pm = \pm \sqrt{\hbar^2 v_F^2 k^2 + \Delta^2}$ accompanied by a flat band $E_0 = 0$ or $\pm \Delta$ according to the sign of U . Pseudo-spin one systems have special matching conditions for the wave functions. In the low-energy regime, it is only necessary to consider the $n = 0$ term in the expansion (24). Although the spinor in the Schrödinger equation for pseudo-spin one systems possesses three components $\Psi(\mathbf{r}) = (u_1(\mathbf{k}), u_2(\mathbf{k}), u_3(\mathbf{k}))e^{-i\mathbf{k}\cdot\mathbf{r}}$, the matching conditions in Eq. (30) involve an effective spinor of two components as

$$\mathbf{w}(\mathbf{k}_{\text{in}/r/t}) = (u_1(\mathbf{k}_{\text{in}/r/t}) + u_3(\mathbf{k}_{\text{in}/r/t}), u_2(\mathbf{k}_{\text{in}/r/t})). \quad (74)$$

For npn bipolar junctions, the configuration (i, j) with $i, j = -1, 0, 1$ denotes the position of the flat band in the regions I and II. Eq. (42) gives the transmission, where

the wave vectors $\mathbf{k}_{\text{in}/r/t}$ in the interface are related to the scattering angles $\theta_{\text{in}/r/t}$

$$\mathbf{k}_{\text{in}/r/t} = \frac{\sqrt{[E - V(x)]^2 - \Delta^2}}{\hbar v_F} (\cos \theta_{\text{in}/r/t}, \sin \theta_{\text{in}/r/t}). \quad (75)$$

The conservation of energy and the y -component of the wave vector allow us to establish the reflection and Snell's law

$$\begin{aligned} \theta_r &= \theta_{\text{in}}, \\ \sin \theta_t &= ss' \frac{\sqrt{E^2 - \Delta^2}}{\sqrt{(E - V)^2 - \Delta^2}} \sin \theta_{\text{in}}, \end{aligned} \quad (76)$$

where s and s' are the band indices in regions I and II, respectively. In this way, transmission is a function of incidence angle θ_{in} , energy E , and the potential height V of the bipolar junction.

In Fig. 12, we showed this transmission for the systems (i, j) . Super-Klein tunneling appears when the focusing energy condition $E = V/2$ is reached for the configuration $(0, 0)$, as shown in Fig. 12(a). The unique configurations for the emergence of super-Klein tunneling are $(0, 0)$, $(-1, 1)$ and $(1, -1)$, corresponding to flat band in the middle band gap, and asymmetric location touching dispersive bands, as shown in Fig. 12(c). These results have pointed out that not only massless particles present super-Klein tunneling, but also massive pseudo-spin one particles.

Further junction configurations with $(0, 1)$, $(1, 0)$, $(0, -1)$, and $(-1, 0)$, the super-Klein tunneling is absent, as seen in Fig. 12(b) and (c). Regardless of the flat band location inside the band gap, the limit of massless particles appears when $E \gg \Delta$, and therefore, the transmission of massive particles is very similar to the massless case [19]. Klein tunneling occurs for a wide range of θ_{in} , which is a distinctive feature of pseudospin-one particles. The effect of flat band location begins to be relevant for energies near the band gap, by considering propagation modes in the range $|E_c| < E < |V| - \Delta$ and $E > |V| + \Delta$, and incidence angle range $-\theta_c \leq \theta_{\text{in}} \leq \theta_c$, where $\theta_c = \arcsin(|E - V|/E)$ is the critical angle.

Most of the pn junctions based on massive pseudo-spin 1 particles have Klein and super-Klein tunneling in contrast to pseudo-spin 1/2 particles [275]. In Fig. 12(c), we compare the transmission of massive pseudospin-one particles as a function of E for the focusing condition $V = 2E$. In the case of massless particles, Klein tunneling is independent of the energy by the conservation of pseudo-spin in $\theta_{\text{in}} = 0$. The transmission probability is the same for the configurations $(-1, -1)$ and $(1, 1)$. Therefore, the flat band location does not affect the transmission under normal incidence in these configurations, but modifies the transmission when $\theta_{\text{in}} \neq 0$. Fabry-Pérot resonances emerge independent on the flat band location.

Super-Klein tunneling of pseudo-spin 1/2 systems

The existence of super-Klein tunneling can also be observed in pseudo-spin-1/2 systems [20]. In the model presented here, the electrostatic barrier does not possess translational invariance; instead, it is realized as a tunable chain of scatterers. The emergence of super-Klein tunneling in this framework can be attributed to its correspondence with a free-particle model, established through a supersymmetric transformation.

In quantum field theory, supersymmetric transformations, known as supercharges, convert bosons into fermions and vice versa. Supersymmetric quantum mechanics was introduced in [276] as a simplified framework for realizing the supersymmetric algebra and exploring the spontaneous breaking of supersymmetry.

Within this model, the supersymmetric Hamiltonian is constructed as a diagonal operator

$$H_{\text{SUSY}} = \begin{pmatrix} H_1 & 0 \\ 0 & H_0 \end{pmatrix}$$

and supercharges are given as

$$Q = \begin{pmatrix} 0 & L \\ 0 & 0 \end{pmatrix}, \quad Q^\dagger = \begin{pmatrix} 0 & 0 \\ L^\dagger & 0 \end{pmatrix}.$$

They satisfy

$$[H, Q] = [H, Q^\dagger], \quad \{Q, Q^\dagger\} = H_{\text{SUSY}}. \quad (77)$$

In this framework, the supercharges do not relate bosons and fermions, they rather provide mapping between two orthogonal states of H_{SUSY} corresponding to its degenerate eigenvalue.

Today, the framework is used mainly to generate new exact solvable models based on existing ones [277, 278]. It is based on the supersymmetric (SUSY) transformation L , which intertwines the operator H_0 , whether it is a Schrödinger or Dirac operator of a known model, with a new operator H_1 that defines the transformed quantum system [279].

The commutator (77) implies in particular the following equality

$$LH_0 = H_1L, \quad (78)$$

that is called the intertwining relation for H_0 and H_1 . It reflects the fact that the eigenstates of H_0 can be mapped into the eigenstates of H_1 by L .

The intertwining operator L is known for a long time in the analysis of differential equations as Darboux transformation, see e.g. [278] and references therein. The intertwining relations for the stationary one-dimensional Dirac equation were discussed in [280], for the non-stationary one in [281].

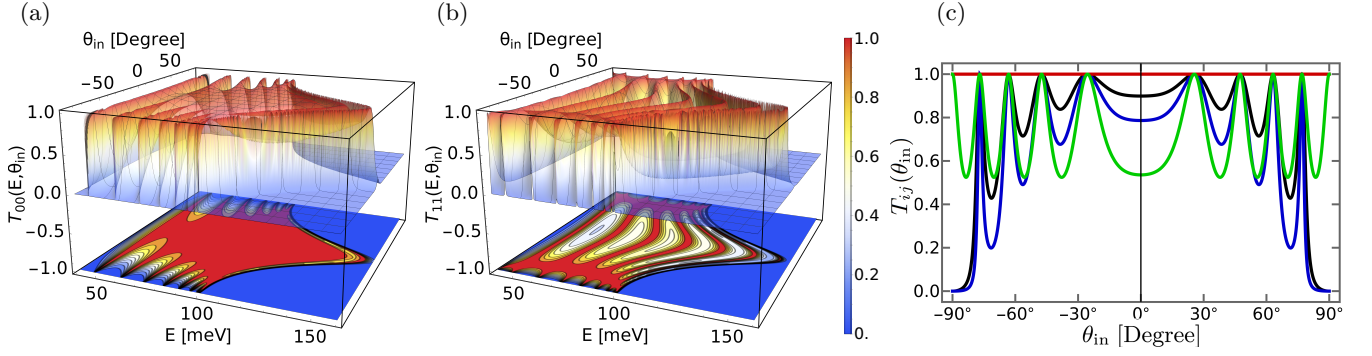


Figure 12. (a) and (b) Interband transmission of massive pseudo-spin one particles as a function of incidence angle θ_{in} and energy E for the configurations (0,0) and (1,1), where the flat band is located at the middle of the band gap and touching the conduction band, respectively. (c) Interband transmission for the focusing condition $V = 2E = 200$ meV as a function of incidence angle. Only the configurations $(-1, 1)$, $(1, -1)$, and $(0, 0)$ (red line) present super-Klein tunneling of massive pseudo-spin one particles. Another curves correspond to the configuration $(1, 0)$ in black, $(1, 1)$ and $(-1, -1)$ in green, and $(-1, 0)$ in blue.

Let us briefly review the framework of non-stationary supersymmetric transformation for 1 + 1D Dirac operators. The Hamiltonian of the initial system is given in the following form

$$H_0\psi = (i\partial_t - i\sigma_2\partial_z - \mathbf{V}_0(z, t))\psi = 0, \quad (79)$$

where $\mathbf{V}_0(z, t)$ is a generic hermitian matrix whose entries can depend both on the spatial coordinate z and on the time coordinate t . We assume that we know two solutions ψ_1 and ψ_2 of the Eq. (79). We compose a 2×2 matrix whose columns correspond to the solutions, $\mathbf{u} = (\psi_1, \psi_2)$. By definition, the matrix satisfies

$$H_0\mathbf{u} = 0. \quad (80)$$

Then we can define the operators L and H_1 with the use of the matrix \mathbf{u} ,

$$\begin{aligned} L &= \partial_z - \mathbf{u}_z\mathbf{u}^{-1}, \quad L^\dagger = -\partial_z - (\mathbf{u}^\dagger)^{-1}\mathbf{u}_z^\dagger, \\ H_1 &= H_0 - i[\sigma_2, \mathbf{u}_z\mathbf{u}^{-1}] \\ &= i\partial_t - i\sigma_2\partial_z - \mathbf{V}_0(z, t) - \mathcal{V}_1^{(1)}(z, t)\sigma_1 - \\ &\quad \mathcal{V}_3^{(1)}(z, t)\sigma_3. \end{aligned} \quad (81)$$

The operators satisfy the intertwining relation (78). The operator H_1 has the new term $i[\sigma_2, \mathbf{u}_z\mathbf{u}^{-1}]$ that can be non-hermitian or singular. Either of these characteristics would compromise the possibility to consider it as the Hamiltonian of the new physical system. The properties of the new potential in H_1 depend on the choice of \mathbf{u} . Its proper selection leading to hermitian and singularity-free operator H_1 can be demanding.

Let us present the case where judicious choice of the matrix \mathbf{u} provides us with a physically acceptable Hamiltonian H_1 . We fix H_0 as the free-particle Hamiltonian,

$$H_0\psi = (i\partial_t - i\sigma_2\partial_z - m\sigma_3)\psi = 0. \quad (82)$$

Its straightforward to find its explicit solutions,

$$\psi_\pm(z, t) = e^{\pm kz} \left(\mp \frac{m \cosh(\omega t) + i\omega \sinh(\omega t)}{k}, \cosh(\omega t) \right)^T, \quad (83)$$

where $k = \sqrt{\omega^2 + m^2}$ and ω are real constants. We fix the following solution $H\psi_1 = 0$,

$$\psi_1(z, t) = \frac{1}{2} (\psi_+(z, t) + \psi_-(z, t)), \quad (84)$$

and compose the matrix \mathbf{u} in this specific manner,

$$\mathbf{u} = (\psi_1, \sigma_1\psi_1). \quad (85)$$

Then the intertwining operator L has the following explicit form

$$\begin{aligned} L &= \partial_z - \frac{1}{2D_1} \left(\frac{\omega^2 \sinh(2kz)}{k} \sigma_0 - 2m \cosh^2(\omega t) \sigma_1 \right. \\ &\quad \left. + \omega \sinh(2\omega t) \sigma_2 \right), \end{aligned} \quad (86)$$

Here, we abbreviated $D_1(z, t) = (m^2 + k^2 \cosh(2\omega t) + \omega^2 \cosh(2kz))/2k^2$. We can construct the new Dirac operator H_1 from the relation (81),

$$\begin{aligned} H_1 &= i\partial_t - i\sigma_2\partial_z - m\sigma_3 \\ &\quad + \frac{4mk^2 \cosh^2(\omega t)}{m^2 + k^2 \cosh(2\omega t) + \omega^2 \cosh(2kz)} \sigma_3. \end{aligned} \quad (87)$$

It is intertwined with H_0 by L via the Eq. (78). The potential term represents a fluctuation of the constant mass, exponentially localized both in time and space. In contrast with the original, free-particle system (82), the new system possesses two solutions which are localized in space-time, see [20].

The derived system described by H_1 is 1 + 1 dimensional. It can be converted into a stationary planar system by the means of Wick rotation. It is facilitated by the following change of the coordinates

$$z = ix, \quad \partial_z = -i\partial_x, \quad t = y. \quad (88)$$

Rewriting the equation (79) in the new coordinates, multiplying it from the left by σ_3 and applying an additional gauge transformation $\mathbf{U} = e^{i\frac{\pi}{4}\sigma_1}$, we obtain a stationary two-dimensional equation at zero energy,

$$\begin{aligned} \tilde{H}_0(x, y)\tilde{\psi}(x, y) &= -\mathbf{U}\sigma_3 H_0(ix, y)\mathbf{U}^{-1}\tilde{\psi}(x, y) \\ &= (-i\sigma_1\partial_x - i\sigma_2\partial_y + \\ &\quad \tilde{\mathbf{V}}_0(x, y))\mathbf{U}\psi(ix, y) \\ &= 0. \end{aligned} \quad (89)$$

The potential term is $\tilde{\mathbf{V}}_0(x, y) = \mathbf{U}\sigma_3\mathbf{V}_0(ix, y)\mathbf{U}^{-1}$. The solutions $\psi(z, t)$ of (79) transform into the solutions $\tilde{\psi}(x, y)$ of (89),

$$\tilde{\psi}(x, y) = \mathbf{U}\psi(ix, y). \quad (90)$$

Now, suppose that two 1 + 1-dimensional operators are related by the intertwining relation (78). The Wick rotation, accompanied by the additional transformations, converts the intertwining relation into the following form

$$\tilde{L}_1(x, y)\tilde{H}_0(x, y) = \tilde{H}_1(x, y)\tilde{L}_2 \quad (91)$$

where the operators

$$\begin{aligned} \tilde{L}_1(x, y) &= \mathbf{U}\sigma_3 L(ix, y)\sigma_3\mathbf{U}^{-1}, \\ \tilde{L}_2(x, y) &= \mathbf{U}L(ix, y)\mathbf{U}^{-1}. \end{aligned} \quad (92)$$

The equality (91) differs from the standard intertwining relation by using two different intertwining operators (92). It allows us to map the solutions of $\tilde{H}_0(x, y)\psi_0(x, y) = 0$ into the solutions of $\tilde{H}_1(x, y)\psi_1(x, y) = 0$,

$$\tilde{H}_0(x, y)\psi_0(x, y) = 0 \implies \tilde{H}_1(x, y)\tilde{L}_2(x, y)\psi_0(x, y) = 0 \quad (93)$$

The Wick rotation transforms the free-particle Dirac operator (82) into the two-dimensional Hamiltonian of a massless particle,

$$\tilde{H}_0 = -i\sigma_1\partial_x - i\sigma_2\partial_y + m\sigma_0. \quad (94)$$

Following (89), the mass term of (87) is converted into the electrostatic potential. We get this stationary equation,

$$\tilde{H}_1\tilde{\psi}(x, y) = \left(-i\sigma_2\partial_y - i\sigma_1\partial_x + \tilde{V}(x, y)\sigma_0\right)\tilde{\psi}(x, y) = 0, \quad (95)$$

where the potential term is

$$\tilde{V}(x, y) = m - \frac{4mk^2 \cosh^2(\omega y)}{m^2 + k^2 \cosh(2\omega y) + \omega^2 \cos(2kx)}. \quad (96)$$

For large values of y , the function rapidly approaches a constant, $\lim_{y \rightarrow \pm\infty} \tilde{V}(x, y) = -m$. To account for this asymptotic behavior, we subtract the limiting value from the electrostatic potential and interpret it as a contribution to the fermion's energy. This leads us to define a modified potential $\mathcal{V}_A = \tilde{V}(x, y) + m$, that reads explicitly

$$\begin{aligned} \mathcal{V}_A(x, y) & \\ &= -\frac{4m\omega^2 \sin^2(kx)}{m^2 + k^2 \cosh(2\omega y) + \omega^2 \cos(2kx)}. \end{aligned} \quad (97)$$

It asymptotically approaches zero as $|y|$ becomes large. Its sign is determined by the sign of m , and it exhibits periodicity in x . Moreover, it is an even function under spatial reflection.

It creates a narrow electrostatic potential resembling a grating or a comb; see Fig. 13. Substituting (97) into (95), we get the stationary equation for energy $E = m$,

$$(-i\sigma_1\partial_x - i\sigma_2\partial_y + \mathcal{V}_A(x, y)\sigma_0)\tilde{\psi}(x, y) = m\tilde{\psi}(x, y). \quad (99)$$

We fix the wave vector \mathbf{k} for an incoming plane wave as follows

$$k_x = m \sin \phi, \quad k_y = m \cos \phi, \quad \phi = (-\pi/2, \pi/2). \quad (100)$$

Then the free-particle solutions of $\tilde{H}_0\tilde{\psi}_\phi(x, y) = 0$ can be written as

$$\tilde{\psi}_\phi(x, y) = e^{im(\sin \phi x + \cos \phi y)} \begin{pmatrix} 1 \\ -ie^{-i\phi} \end{pmatrix}. \quad (101)$$

The parameter ϕ corresponds to the incidence angle of the plane wave. The spinor $\tilde{\psi}_\phi$ can be transformed into the scattering solution of Eq.(99),

$$(-i\sigma_1\partial_x - i\sigma_2\partial_y + \mathcal{V}_A(x, y))\tilde{L}\tilde{\psi}_\phi(x, y) = m\tilde{L}\tilde{\psi}_\phi(x, y). \quad (102)$$

For large $|y|$, the operator \tilde{L} has the following asymptotic form

$$\tilde{L} \sim \begin{cases} -i\partial_x + m\sigma_1 - \omega\sigma_3, & y \rightarrow -\infty, \\ -i\partial_x + m\sigma_1 + \omega\sigma_3, & y \rightarrow \infty. \end{cases} \quad (103)$$

Hence, the action of \tilde{L} on $\tilde{\psi}_\phi$ is

$$\lim_{y \rightarrow \pm\infty} \tilde{L}\tilde{\psi}_\phi = e^{im(\sin \phi x + \cos \phi y)} (\pm\omega - im \cos \phi) \begin{pmatrix} 1 \\ ie^{-i\phi} \end{pmatrix}. \quad (104)$$

The relation (104) reveals that there is no reflection of the Dirac fermions on the potential, independently on the incidence angle, provided that the particle has energy $E = m$. Therefore, the system possesses super-Klein tunneling. The scattering state $\tilde{L}\tilde{\psi}_\phi$ accumulates the phase

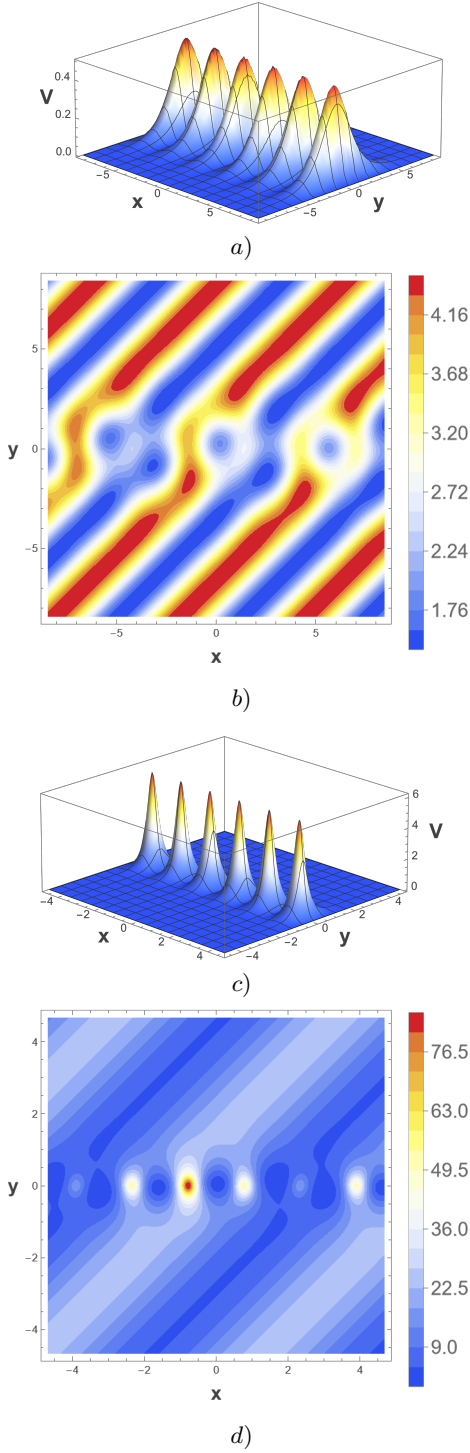


Figure 13. (color online) The potential term $\mathcal{V}_A(x, y)$ (a) and c) and the density of probability b) and d) of a linear combination of asymptotically plane-wave solutions (106). There is $\omega = 1.75$ in a), b) and $\omega = 0.5$ in c) and d). We fixed $m = -1$ and $\phi_1 = 0$, $\phi_2 = \frac{\pi}{2}$ in all plots.

shift when passing through the barrier,

$$\lim_{y \rightarrow +\infty} \tilde{L}\tilde{\psi}_\phi = \frac{\omega - im \cos \phi}{-\omega - im \cos \phi} \left(\lim_{y \rightarrow -\infty} \tilde{L}\tilde{\psi}_0 \right). \quad (105)$$

The phase shift depends both on the potential (determined by the values of m and ω) and on the incidence angle ϕ . It is symmetric with respect to $\phi \rightarrow -\phi$ which is to be expected as the potential term is symmetric with respect to $x \rightarrow -x$. The phase shift changes the interference pattern of a linear combination of the plane waves. Taking the sum of two plane waves with incidence angles ϕ_1 and ϕ_2 ,

$$F_A(x, y, \phi_1, \phi_2) = \tilde{L}\tilde{\psi}_0(x, y, \phi_1) + \tilde{L}\tilde{\psi}_0(x, y, \phi_2), \quad (106)$$

the interference pattern gets slightly shifted along x axis when passing through the potential barrier, see Fig. 13 for illustration.

Valley-cooperative Klein tunneling in Kekulé graphene superlattices

Valley-cooperative Klein tunneling is a variant of the conventional Klein tunneling in graphene that arises when the two Dirac cones at the K^+ and K^- valleys possess different Fermi velocities [108]. An ideal platform for observing this effect is provided by the Kekulé-Y graphene superlattice [143, 150, 282–286]. Following the procedure of tight-binding approach to nearest neighbors outlined in Eqs. (1) to (8), the Bloch Hamiltonian of Kekulé-Y graphene, with six Carbon atoms in the unit cell as illustrated in Fig. 14(a), can be written as

$$H_{\text{Kek-Y}}^{\text{B}}(\mathbf{k}) = \begin{pmatrix} 0 & t'e^{ik \cdot \delta_2} & 0 & te^{ik \cdot \delta_3} & 0 & te^{ik \cdot \delta_1} \\ t'e^{-ik \cdot \delta_2} & 0 & t'e^{-ik \cdot \delta_3} & 0 & t'e^{-ik \cdot \delta_1} & 0 \\ 0 & t'e^{ik \cdot \delta_3} & 0 & te^{ik \cdot \delta_1} & 0 & te^{ik \cdot \delta_2} \\ te^{-ik \cdot \delta_3} & 0 & te^{-ik \cdot \delta_1} & 0 & te^{-ik \cdot \delta_2} & 0 \\ 0 & t'e^{ik \cdot \delta_1} & 0 & te^{-ik \cdot \delta_2} & 0 & te^{ik \cdot \delta_3} \\ te^{-ik \cdot \delta_1} & 0 & te^{-ik \cdot \delta_2} & 0 & te^{-ik \cdot \delta_3} & 0 \end{pmatrix}. \quad (107)$$

Upon diagonalization of this Hamiltonian, the band structure exhibits two Dirac cones with different Fermi velocities at the center of the first Brillouin zone, as seen in Fig. 14(b). The original first Brillouin zone of graphene is folded, yielding a reduced hexagonal Brillouin zone, where energy bands are mapped onto the Γ point. As illustrated in Fig. 14(c), the energy contours for the red conduction band displayed in Fig. 14(b) indicate that this Dirac cone is isotropic in the vicinity of the Γ point. Expanding the Bloch Hamiltonian of Eq. (107) around this point and neglecting the upper and lower

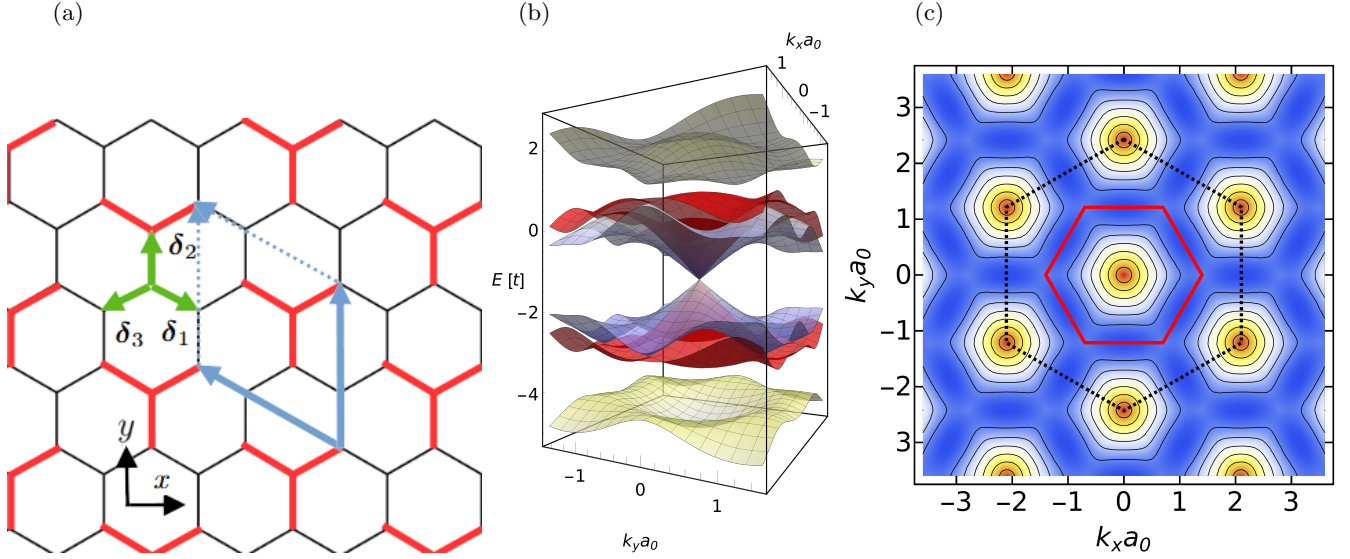


Figure 14. (a) Lattice structure of Kekulé-Y graphene. The periodic distortion in Y is indicated by the hopping parameter t' and the simple one by t . The unit cell contains six Carbon atoms. (b) The electronic band structure from the eigenenergies of the Bloch Hamiltonian in Eq. (107) as a function of wave vector \mathbf{k} . Two Dirac cones appear in the center of the first Brillouin zone with Fermi velocities $v_\tau \pm v_\sigma$. (c) Energy contours of the red conduction band in (b).

bands leads to an effective 4×4 continuum Hamiltonian, valid to linear order in momentum $\mathbf{p} = \hbar\mathbf{k}$

$$H_{\text{Kek-Y}} = \begin{pmatrix} 0 & v_\sigma p_- & v_\tau p_- & 0 \\ v_\sigma p_+ & 0 & 0 & v_\tau p_- \\ v_\tau p_+ & 0 & 0 & v_\sigma p_- \\ 0 & v_\tau p_+ & v_\sigma p_+ & 0 \end{pmatrix}, \quad (108)$$

where v_σ is the Fermi velocity and v_τ quantifies the periodic distortion of the Kekulé graphene. We define the linear momentum components as $p_\pm = p_x \pm ip_y$. The dispersion relations have a simple linear form $E_{\nu,s} = s(v_\sigma + \nu v_\tau)p$, where $s = \pm 1$ and $\nu = \pm 1$ are the band and valley index, respectively, and $p = \sqrt{p_x^2 + p_y^2}$ is the magnitude of linear momentum. The velocities v_τ and v_σ are related with the hopping parameters t and t' [286, 287].

Using the wave functions (25) and (26) for a pn junction, we compute the transmission coefficient via Eq. (36), and presents the results in Fig. 15. The incident state is prepared with equal weights 50% in the K^+ and K^- valleys. At normal incidence, perfect tunneling appears as a consequence of pseudospin conservation. For oblique incidence, $\theta \neq 0^\circ$, electrons have non-zero probabilities for the reflection and transmission in each valleys. Remarkably, an unconventional transmission behavior occurs at normal incidence. Although back-scattering is completely suppress ($R^\nu = 0$), the transmitted current is not equally distributed between the two valleys. Instead, for the ratio $v_\tau/v_\sigma = 0.2$, the transmitted fractions are 0.6 and 0.4 in the K^- and K^+ valleys, respectively. This means that 10% of the electrons initially in the K^- valley undergo a valley-flip, enabling cooperative

transmission across the interface without backscattering. We refer to this counterintuitive transport mechanism as valley-cooperative Klein tunneling [108].

The valley flip process is controlled only by the Kekulé distortion. Increasing the velocity v_τ , the difference of $T_+ - T_-$ under normal incidence also increases, as shown in Fig. 15. This effect is due to the Kekulé distortion and the conservation of the pseudospin, which is independent of the Fermi level and electrostatic potential. To analyze the valley-cooperative Klein tunneling, we calculate the transmission probabilities for normal incidence and weights a^\pm

$$T^\pm(0) = \frac{(v_\sigma \pm v_\tau)|a^\pm|^2}{\sum_\nu (v_\sigma + \nu v_\tau)|a^\nu|^2}, \quad (109)$$

where the pseudospin angles are $\phi_i^- = \phi_i^+ = 0$, $\phi_r^- = \phi_r^+ = \pi$, and $\phi_t^- = \phi_t^+ = (s - s')\pi/2$. For the reflection coefficients, we have $R^\pm = 0$. For $|a^\nu|^2 = 0.5$ the Eq. (109) can be simplified to $T^\pm(0) = \frac{1}{2}(1 \pm \frac{v_\tau}{v_\sigma})$. Clearly, we observe that $T^-(0) + T^+(0) = 1$. We recover the conventional Klein tunneling in graphene making $v_\tau = 0$, and as expected, unpolarized current under normal incidence crosses perfectly the electrostatic potential [3, 4]. The extreme case $v_\sigma = v_\tau$ indicates that all the electrons in the K^- valley perform a valley-flip to cross perfectly the junction, resulting in a fully valley polarized current. This behavior is evidenced in Fig. (15) for different Kekulé-Y distortions v_τ/v_σ . Moreover, $v_\sigma = v_\tau$ merges the conduction and valence bands in the K^- valley to a flat band, giving rise to super-Klein tunneling, which is a typical phenomenon in the scattering of pseudospin-one particles [13, 16, 17, 19, 20, 36, 37, 39, 47, 48, 96].

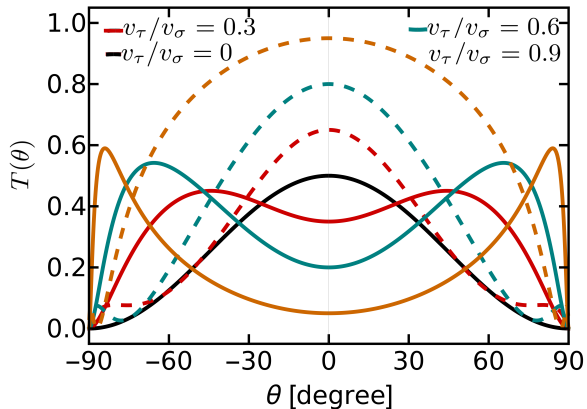


Figure 15. Electron transmission in pn junctions of Kekulé-Y graphene as a function of incidence angle θ . The different curves, solid and dashes with the same color, correspond to the valleys K^+ and K^- , respectively. By increasing the Kekulé distortion, which is quantified through the ratio v_τ/v_σ , the valley-flip is more evident for normal incidence. The conservation of pseudo-spin guarantees that $T^+(0) + T^-(0) = 1$.

When chiral symmetry is broken, massive Dirac fermions exhibit a finite reflection probability. However, the sum of probabilities $R^+ + T^+$ remains greater than 0.5. If the band gap is valley-dependent, the junction works as a perfect valley filter. In the pseudo-ultra-relativistic regime (i.e. at high energies), the transmission displays the same behavior as in the gapless case [108]. For normal incidence, both reflection and transmission are constant and independent of the energy due to pseudospin conservation. In particular, the valley-flip mechanism underlying valley-cooperative Klein tunneling persists even when the chiral symmetry is broken in both valleys, since the valley-flip process depends solely on the Fermi velocities $v_\sigma + \nu v_\tau$.

To quantify the degree of polarization P in KekGr pn junctions, we define

$$P = \frac{\langle T^+ \rangle - \langle T^- \rangle}{\langle T^+ \rangle + \langle T^- \rangle}, \quad (110)$$

where $\langle T^\nu \rangle$ is the angular averaged transmission. The polarization in junctions for massless Dirac fermions remains almost constant for intraband transmission ($E > V$) and has the approximated value of $P \approx v_\tau/v_\sigma = 0.1$. This asymptotic value of P remains approximately constant with the smoothness of the junction, and it is a signature of the valley-flip process that may be detected experimentally. Fully valley polarized current flow is achieved by breaking the chiral symmetry. The polarization can be changed by tuning the Fermi energy within the different gaps of the valleys, making these systems a perfect valley switch.

CONCLUSIONS AND FINAL REMARKS

Klein tunneling is a robust transport phenomenon that persists across a wide variety of physical systems and can be understood beyond the framework of the Dirac equation. In this review, we presented a unifying perspective based on a tight-binding approach, in which periodic systems are naturally described by Bloch Hamiltonians. Within this framework, the matching conditions at interfaces depend on the underlying crystal properties and may differ from the conventional continuity of the wave function and its derivative prescribed by the Schrödinger equation, particularly when higher-order terms in the wave vector are taken into account.

Most importantly, we identified that the emergence of Klein and anti-Klein tunneling is governed by the conservation of an effective pseudo-spin one-half imposed by the matching conditions. This identification broadens the range of systems in which these phenomena can arise, from synthesized materials such as graphene, borophene, and phosphorene, as well as artificial lattices, among them, phononic and photonic crystals [8, 288, 289]. Moreover, Klein tunneling is not restricted to electronic systems, but also it can emerge for acoustic and electromagnetic waves, extending well beyond the Dirac paradigm [9, 288].

Historically, Klein tunneling was originally predicted by Oskar Klein within the context of the Dirac equation [1]. Remarkably, perfect tunneling is also possible for spinless particles governed by the Klein-Gordon equation [26]. The introduction of the angle $\gamma(\mathbf{k}_{\text{in}}, \mathbf{k}_{\text{t}})$ in Eq. (51) enabled us to identify Klein tunneling independently of the specific nature of the pseudo-spin, whether originating from sublattice, intrinsic spin, or other internal degrees of freedom [181]. For instance, massive pseudo-spin-one particles obey the conservation of an effective and reduced pseudo-spin one-half given by the state $\mathbf{w}(\mathbf{k}_{\text{in}/\text{r}/\text{t}})$, as shown in Eq. (74). Similarly, spinless particles acquire an effective pseudo-spin one-half through scattering at an interface. In general, when an incoming wave impinges on an interface, it partially reflects and partially transmits. Under the matching conditions, an effective spinor $\mathbf{w}(\mathbf{k})$ can be constructed, as defined in Eq. (30). The appearance of Klein or anti-Klein tunneling is therefore strongly dictated by the intrinsic properties of the system and is independent of the applied electrostatic potential. We discussed the diversity of Klein tunneling phenomena across systems of different dimensionalities. In Su-Schrieffer-Heeger chains, the topological phase transition leads to an interchange between Klein tunneling in the trivial phase and topological phase for interband and intraband regimes.

Anisotropic materials, such as borophene and strained graphene, gives rise to anomalous Klein tunneling [31, 256, 257], where perfect transmission occurs at oblique

incidence rather than normal incidence. The angular deviation of this anomalous tunneling depends on the Fermi velocity tensor components, as shown in Eq. (67). Despite its fundamental importance, Klein tunneling has not yet been experimentally realized in high-energy physics. Its first experimental observation occurred in condensed-matter systems followed by the discovery of graphene [7, 290]. More recently, experimental realizations in acoustic and phononic crystals have revealed Klein tunneling to be an omnipresent consequence of the wave nature of matter and classical fields [8, 10, 97]. Several related phenomena, including super-Klein tunneling in massive pseudo-spin-one and one-half systems [19, 20], anti-super-Klein tunneling [111, 119, 259], one-dimensional chains [181], and valley-cooperative Klein tunneling [108], remain experimentally unexplored. Nevertheless, the rapid development of artificial lattices, such as elastic metamaterials [181, 231, 291], topoelectrical circuits [292–294], ultracold atoms in optical lattices [295, 296], and photonic [211, 213, 216, 289, 297, 298] and phononic [8, 10, 11, 40, 157, 299–301] crystals provides promising platforms for realizing these unconventional effects. Finally, Klein tunneling holds significant potential for technological applications, including ultrafast transistor operations [302], high-efficiency electron-optics devices, and advanced wave-manipulation components based on collimators [27, 107], Veselago and super-diverging lenses [132].

ACKNOWLEDGMENTS

Y.B.-O. gratefully acknowledges financial support from UNAM-PAPIIT project IA 102125.

* ybetancur@fisica.unam.mx

† monsi@fisica.unam.mx

‡ jakubsky@ujf.cas.cz

- [1] Klein O 1929 Zeitschrift für Physik **53** 157–165 ISSN 1434-601X
- [2] Beenakker C W J 2008 Reviews of Modern Physics **80** 1337–1354 ISSN 1539-0756
- [3] Allain P E and Fuchs J N 2011 The European Physical Journal B **83** 301–317 ISSN 1434-6036
- [4] Katsnelson M I, Novoselov K S and Geim A K 2006 Nature Physics **2** 620–625 ISSN 1745-2481
- [5] He P and Li Z 2020 (*Preprint* 2004.04885)
- [6] Landauer R and Martin T 1994 Reviews of Modern Physics **66** 217–228 ISSN 1539-0756
- [7] Young A F and Kim P 2009 Nature Physics **5** 222–226 ISSN 1745-2481
- [8] Jiang X, Shi C, Li Z, Wang S, Wang Y, Yang S, Louie S G and Zhang X 2020 Science **370** 1447–1450 ISSN 1095-9203
- [9] Zhang Z, Feng Y, Li F, Koniakhin S, Li C, Liu F, Zhang Y, Xiao M, Malpuech G and Solnyshkov D 2022 Physical Review Letters **129** 233901 ISSN 1079-7114
- [10] Zhu Y, Merkel A, Cao L, Zeng Y, Wan S, Guo T, Su Z, Gao S, Zeng H, Zhang H and Assouar B 2023 Applied Physics Letters **122** ISSN 1077-3118
- [11] Wu H, He H, Dong Z, Ye L, Deng W, Ke M and Liu Z 2024 Physical Review Applied **21** 034026 ISSN 2331-7019
- [12] Bercieux D, Urban D F, Grabert H and Häusler W 2009 Physical Review A **80** 063603 ISSN 1094-1622
- [13] Shen R, Shao L B, Wang B and Xing D Y 2010 Physical Review B **81** 041410 ISSN 1550-235X
- [14] Dóra B, Kailasvuori J and Moessner R 2011 Physical Review B **84** 195422 ISSN 1550-235X
- [15] Lan Z, Goldman N, Bermudez A, Lu W and Öhberg P 2011 Physical Review B **84** 165115 ISSN 1550-235X
- [16] Urban D F, Bercieux D, Wimmer M and Häusler W 2011 Physical Review B **84** 115136 ISSN 1550-235X
- [17] Xu H Y and Lai Y C 2016 Physical Review B **94** 165405 ISSN 2469-9969
- [18] Bercieux D, Dutta O and Rico E 2017 Annalen der Physik **529** 1600262
- [19] Betancur-Ocampo Y and Gupta V 2017 Journal of Physics: Condensed Matter **30** 035501 ISSN 1361-648X
- [20] Contreras-Astorga A, Correa F and Jakubský V 2020 Physical Review B **102** 115429 ISSN 2469-9969
- [21] Cunha S M, da Costa D R, Felix L C, Chaves A and Pereira J M 2020 Physical Review B **102** 045427 ISSN 2469-9969
- [22] Chen Y R, Xu Y, Wang J, Liu J F and Ma Z 2019 Physical Review B **99** 045420 ISSN 2469-9969
- [23] Wang J, Liu J F and Ting C S 2020 Physical Review B **101** 205420 ISSN 2469-9969
- [24] Hao L 2021 Physical Review B **104** 195155 ISSN 2469-9969
- [25] Liu H L, Wang J and Liu J F 2022 Physica E: Low-dimensional Systems and Nanostructures **144** 115454 ISSN 1386-9477
- [26] Kim S and Kim K 2019 Physical Review B **100** 104201 ISSN 2469-9969
- [27] Wang J and Liu J F 2022 Physical Review B **105** 035402 ISSN 2469-9969
- [28] Liu H L, Hao L, Wang J and Liu J F 2023 Physical Review B **108** 115141 ISSN 2469-9969
- [29] Duan W 2023 Physical Review B **108** 155428 ISSN 2469-9969
- [30] Kim K 2019 Results in Physics **12** 1391–1394 ISSN 2211-3797
- [31] Betancur-Ocampo Y 2018 Physical Review B **98** 205421 ISSN 2469-9969
- [32] Jakubský V and Zelaya K 2023 Physica E: Low-dimensional Systems and Nanostructures **152** 115738 ISSN 1386-9477
- [33] Zeng W and Shen R 2022 New Journal of Physics **24** 043021 ISSN 1367-2630
- [34] Korol A M, Medvid N V and Sokolenko A I 2018 physica status solidi (b) **255** ISSN 1521-3951
- [35] Crasto de Lima F and Ferreira G J 2020 Physical Review B **101** 041107 ISSN 2469-9969
- [36] Nandy S, Sengupta K and Sen D 2019 Physical Review B **100** 085134 ISSN 2469-9969
- [37] Kim S and Kim K 2020 Physical Review B **101** 165428 ISSN 2469-9969

- [38] Filusch A and Fehske H 2020 The European Physical Journal B **93** ISSN 1434-6036
- [39] Xu H Y, Huang L and Lai Y C 2021 Physical Review Research **3** 013284
- [40] Sirota L 2021 (*Preprint* 2107.04893)
- [41] Majari P 2021 (*Preprint* 2109.03196)
- [42] Chen S G, Kong X, Zhang L L and Gong W J 2024 The Journal of Physical Chemistry Letters **15** 4799–4805 ISSN 1948-7185
- [43] Zhou X 2021 (*Preprint* 2105.11070)
- [44] Oriekhov D O and Voronov S 2021 (*Preprint* 2104.12271)
- [45] Wang X H, Wang J J, Wang J and Liu J F 2021 Physical Review B **103** 195442 ISSN 2469-9969
- [46] Ding Z, Wang D, Lu L, Li M, Tao Y and Huang F 2024 Annals of Physics **471** 169848 ISSN 0003-4916
- [47] Mandhour L and Bouhadida F 2026 Physica E: Low-dimensional Systems and Nanostructures **177** 116424 ISSN 1386-9477
- [48] Mandhour L and Bouhadida F 2020 (*Preprint* 2004.10144)
- [49] Fadil Z, Raorane C J, Jabar A, Mahmoud K H, Alsayyari A A and Kim S C 2025 The European Physical Journal B **98** ISSN 1434-6036
- [50] Liu H L and Wang J 2025 Physica E: Low-dimensional Systems and Nanostructures **165** 116096 ISSN 1386-9477
- [51] Iurov A, Zhemchuzhna L, Gumbs G, Huang D and Fekete P 2022 Physical Review B **105** 115309
- [52] Iurov A, Zhemchuzhna L, Gumbs G, Huang D and Fekete P 2021 (*Preprint* 2112.13458)
- [53] Hao L 2022 Physical Review Materials **6** 034002 ISSN 2475-9953
- [54] Wan L L, Lü X Y, Gao J H and Wu Y 2017 Optics Express **25** 17364
- [55] Graf A and Piéchon F 2021 (*Preprint* 2106.10664)
- [56] Lara T F O, Barros E B, Lima W P, Nascimento J P G, Pereira Jr J M, Pereira T A S and da Costa D R 2025 Nanotechnology **36** 395702 ISSN 1361-6528
- [57] de Lima F C and Fazzio A 2020 Nanoscale, 2021,13, 5270-5274 (*Preprint* 2011.11045)
- [58] Feng H, Liu C, Zhou S, Gao N, Gao Q, Zhuang J, Xu X, Hu Z, Wang J, Chen L, Zhao J, Dou S X and Du Y 2020 Nano Letters **20** 2537–2543
- [59] Hwang Y, Rhim J W and Yang B J 2021 (*Preprint* 2105.14919)
- [60] Banerjee S and Saxena A 2021 Physical Review B **103** 235125
- [61] Han Y K, Seo J W, Yuk T and Sin S J 2022 (*Preprint* 2205.12540)
- [62] Flannigan S, Madail L, Dias R G and Daley A J 2021 (*Preprint* 2101.03819)
- [63] Huhtinen K E and Törmä P 2020 Phys. Rev. B **103**, 220502 (2021) (*Preprint* 2007.05118)
- [64] Zelaya K and Jakubský V 2022 (*Preprint* 2207.04133)
- [65] Liu J, Mao X, Zhong J and Römer R A 2020 Phys. Rev. B **102**, 174207 (2020) (*Preprint* 2004.08042)
- [66] Liu J, Mao X, Zhong J and Römer R A 2021 Annals of Physics **168544** (2021) (*Preprint* 2102.00161)
- [67] Hanafi H, Menz P, McWilliam A, Imbrock J and Denz C 2022 (*Preprint* 2207.01480)
- [68] Mejía-Cortés C, Castillo-Barake J and Molina M I 2020 (*Preprint* 2005.09650)
- [69] Cao X, Chen K and He D 2015 Journal of Physics: Condensed Matter **27** 166003
- [70] Li Y, Tian L, Ma T and Lin H Q 2022 (*Preprint* 2206.03890)
- [71] Ali A K S, Maimistov A I, Porsezian K, Govindarajan A and Lakshmanan M 2020 (*Preprint* 2012.04287)
- [72] Xu Y and Jin G 2014 Physics Letters A **378** 3554–3560
- [73] Whittaker C E, Gulevich D R, Biegańska D, Royall B, Clarke E, Skolnick M S, Shelykh I A and Krizhanovskii D N 2021 Physical Review A **104** 063505
- [74] Lima L 2022 Physica E: Low-dimensional Systems and Nanostructures **115235**
- [75] Dauphin A, Müller M and Martin-Delgado M A 2016 Physical Review A **93** 043611
- [76] Bouzerar G 2021 (*Preprint* 2106.10117)
- [77] Kusdiantara R, Akbar F T, Nuraini N, Gunara B E and Susanto H 2022 Journal of Nonlinear Science **32**
- [78] Román-Cortés D, Fadic G, Cid-Lara C, Guzmán-Silva D, Real B and Vicencio R A 2021 **11**
- [79] Yamazaki K, Ochi M, Ogura D, Kuroki K, Eisaki H, Uchida S and Aoki H 2020 Physical Review Research **2** 033356
- [80] Feng X, Zhang L and Jiang L 2021 Chinese Physics B
- [81] Goldman N, Urban D F and Bercioux D 2011 Physical Review A **83** 063601
- [82] Abramovici G 2021 Eur. Phys. J. B (2021) 94:132 (*Preprint* 2106.14978)
- [83] Pires A 2021 Journal of Magnetism and Magnetic Materials **168941**
- [84] Scafrimuto F, Urbonas D, Becker M A, Scherf U, Mahrt R F and Stöferle T 2021 Communications Physics **4**
- [85] Xia S, Ramachandran A, Xia S, Li D, Liu X, Tang L, Hu Y, Song D, Xu J, Leykam D, Flach S and Chen Z 2018 Physical Review Letters **121** 263902
- [86] Cunha S M, da Costa D R, Pereira J M, Filho R N C, Duppen B V and Peeters F M 2021 Physical Review B **104** 115409
- [87] Dragoman M, Dinescu A, Dragoman D and Comanescu F 2021 Nanotechnology **32** 345203 ISSN 1361-6528
- [88] Guzmán E J, Oubram O, Navarro O and Rodríguez-Vargas I 2023 Physical Review B **107** 045407 ISSN 2469-9969
- [89] Ícaro SF Bezerra and Lima J R 2020 Physica E: Low-dimensional Systems and Nanostructures **123** 114171 ISSN 1386-9477 URL <http://www.sciencedirect.com/science/article/pii/S1386947720306408>
- [90] Wang L G and Zhu S Y 2010 Phys. Rev. B **81**(20) 205444 URL <https://link.aps.org/doi/10.1103/PhysRevB.81.205444>
- [91] Agrawal (Garg) N, Ghosh S and Sharma M 2013 International Journal of Modern Physics B **27** 1341003 (*Preprint* <https://doi.org/10.1142/S0217979213410038>) URL <https://doi.org/10.1142/S0217979213410038>
- [92] Briones-Torres J, Madrigal-Melchor J, Martínez-Orozco J and Rodríguez-Vargas I 2014 Superlattices and Microstructures **73** 98–112 ISSN 0749-6036 URL <https://www.sciencedirect.com/science/article/pii/S0749603614001876>
- [93] Guzmán E J, Navarro O, Oubram O and Rodríguez-Vargas I 2018 Journal of Applied Physics **124** 144305
- [94] Zhang Y, Wang X and Li Y X 2025 Journal of Applied Physics **138** ISSN 1089-7550

- [95] Pang G X, Li Z, Li S Z, Zhang Y Y, Liu J F and Zhang Y C 2025 Physical Review B **111** ISSN 2469-9969
- [96] Wang J and Liu J F 2021 Physical Review B **103** 075419 ISSN 2469-9969
- [97] Zhang Y C 2022 Scientific Reports **12** ISSN 2045-2322
- [98] Wang J J, Liu S, Wang J and Liu J F 2020 Physical Review B **102** 235414 ISSN 2469-9969
- [99] Li F, Zhang Q and Chan K S 2022 Scientific Reports **12** ISSN 2045-2322
- [100] Zhang Y C and Zhu G B 2022 Journal of Physics B: Atomic, Molecular and Optical Physics **55** 065001 ISSN 1361-6455
- [101] Zhang Y C 2022 Chinese Physics B **31** 050311 ISSN 1674-1056
- [102] Wen X P and Niu Z P 2023 Physics Letters A **489** 129157 ISSN 0375-9601
- [103] Betancur-Ocampo Y, Cordourier-Maruri G, Gupta V and de Coss R 2017 Physical Review B **96** 024304 ISSN 2469-9969
- [104] Navarro-Labastida L A and Naumis G G 2023 Physical Review B **107** 155428 ISSN 2469-9969
- [105] Xie D, Gou W, Xiao T, Gadway B and Yan B 2019 npj Quantum Information **5** 55
- [106] Huang Y, Zeng W and Shen R 2023 Physics Letters A **463** 128671 ISSN 0375-9601
- [107] Xu Y, Liu J, Xi B, Zhou X and Liu Y 2023 New Journal of Physics **25** 113002 ISSN 1367-2630
- [108] García S G y, Stegmann T and Betancur-Ocampo Y 2022 Physical Review B **105** 125139 ISSN 2469-9969
- [109] Majari P and Naumis G G 2023 Physica B: Condensed Matter **668** 415238 ISSN 0921-4526
- [110] Septembre I, Solnyshkov D D and Malpuech G 2023 Physical Review B **108** 115309 ISSN 2469-9969
- [111] Betancur-Ocampo Y, Leyvraz F and Stegmann T 2019 Nano Letters **19** 7760–7769 ISSN 1530-6992
- [112] Betancur-Ocampo Y, Paredes-Rocha E and Stegmann T 2020 Journal of Applied Physics **128** ISSN 1089-7550
- [113] Molina-Valdovinos S, Lamas-Martínez K J, Briones-Torres J A and Rodríguez-Vargas I 2022 Journal of Physics: Condensed Matter **34** 195301 ISSN 1361-648X
- [114] Hua J, Wang Z F, Zhu W and Chen W 2024 Physical Review B **109** 115429 ISSN 2469-9969
- [115] Feng C and Scalettar R T 2020 Phys. Rev. B **102**, 235152 (2020) (*Preprint* 2009.05595)
- [116] Sui C, Yuan S, Gao D, Yu D and Jia C 2025 Physical Review B **112** ISSN 2469-9969
- [117] Lee G H, Park G H and Lee H J 2015 Nature Physics **11** 925–929 ISSN 1745-2481
- [118] Chen S, Han Z, Elahi M M, Habib K M M, Wang L, Wen B, Gao Y, Taniguchi T, Watanabe K, Hone J, Ghosh A W and Dean C R 2016 Science **353** 1522–1525 ISSN 1095-9203
- [119] Paredes-Rocha E, Betancur-Ocampo Y, Szpak N and Stegmann T 2021 Physical Review B **103** 045404 ISSN 2469-9969
- [120] Bai K K, Zhou J J, Wei Y C, Qiao J B, Liu Y W, Liu H W, Jiang H and He L 2018 Physical Review B **97** 045413 ISSN 2469-9969
- [121] Sajjad R N and Ghosh A W 2011 Applied Physics Letters **99** ISSN 1077-3118
- [122] Cheianov V V, Fal'ko V and Altshuler B L 2007 Science **315** 1252–1255 ISSN 1095-9203
- [123] Lassaline N, Sørensen C H, Meucci G, Linde S J, Latifi Yaghin K, Nielsen M V, Chau T K, Carrad D J, Bøggild P, Jespersen T S and Booth T J 2025 Nano Letters ISSN 1530-6992
- [124] Ildarabadi F and Power S R 2025 ACS Applied Electronic Materials **7** 10631–10637 ISSN 2637-6113
- [125] Butanov K, Baydjanov M, Yusupov H, Bobojonov K, Yusupov M, Chaves A and Rakhimov K 2025
- [126] Chen X, Weick G, Weinmann D and Jalabert R A 2023 Physical Review B **107** 085420 ISSN 2469-9969
- [127] Li Y, Chan C T and Mazur E 2021 Light: Science & Applications **10**
- [128] Veselago V G 1968 Soviet Physics Uspekhi **10** 509–514 ISSN 0038-5670
- [129] Pendry J B 2000 Physical Review Letters **85** 3966–3969 ISSN 1079-7114
- [130] Betancur-Ocampo Y 2018 Journal of Physics: Condensed Matter **30** 435302 ISSN 1361-648X
- [131] Hills R D Y, Kusmartseva A and Kusmartsev F V 2017 Physical Review B **95** 214103 ISSN 2469-9969
- [132] Heinisch R L, Bronold F X and Fehske H 2013 Physical Review B **87** 155409 ISSN 1550-235X
- [133] Padilla-Ortiz A L, Pisano E, Chávez-Cerda S and Gómez-Correa J E 2025 Applied Optics **64** 1362 ISSN 2155-3165
- [134] Dragoman D and Dragoman M 2024 Solid-State Electronics **211** 108818 ISSN 0038-1101
- [135] Banerjee P S, Marathe R and Ghosh S 2024 Journal of Optics **26** 095602 ISSN 2040-8986
- [136] García-Pomar J L, Cortijo A and Nieto-Vesperinas M 2008 Physical Review Letters **100** 236801 ISSN 1079-7114
- [137] Settnes M, Power S R, Brandbyge M and Jauho A P 2016 Physical Review Letters **117** 276801 ISSN 1079-7114
- [138] Zhai D and Sandler N 2018 Physical Review B **98** 165437 ISSN 2469-9969
- [139] Contreras-Astorga A, Jakubský V and Raya A 2020 Journal of Physics: Condensed Matter **32** 295301 URL <https://doi.org/10.1088/1361-648X/ab7e5b>
- [140] Grujic M M, Tadic M Z and Peeters F M 2014 Physical Review Letters **113** 046601 ISSN 1079-7114
- [141] Chauwin M, Siu Z B and Jalil M B A 2022 Physical Review Applied **17** 024035
- [142] Zhai F, Ma Y and Chang K 2011 New Journal of Physics **13** 083029 ISSN 1367-2630
- [143] Wang J J, Liu S, Wang J and Liu J F 2018 Physical Review B **98** 195436 ISSN 2469-9969
- [144] Prabhakar S, Nepal R, Melnik R and Kovalev A A 2019 Physical Review B **99** 094111 ISSN 2469-9969
- [145] Tan H, Xu Y, Wang J, Liu J F and Ma Z 2020 Journal of Physics D: Applied Physics **54** 105303 ISSN 1361-6463
- [146] Filusch A, Bishop A R, Saxena A, Wellein G and Fehske H 2021 Physical Review B **103** 165114
- [147] Islam S F and Dutta P 2017 Physical Review B **96** 045418
- [148] Parui P and Chittari B L 2025 Physical Review B **112** ISSN 2469-9969
- [149] Niu Z P and Wang S J 2022 Journal of Physics D: Applied Physics **55** 255303 ISSN 1361-6463
- [150] Juan-Juan W and Jun W 2024 Chinese Physics B **33** 017801 ISSN 2058-3834
- [151] Schaibley J R, Yu H, Clark G, Rivera P, Ross J S, Seyler K L, Yao W and Xu X 2016 Nature Reviews Materials **1** ISSN 2058-8437

- [152] Vanderstraeten E and Vande Ginste D 2024 Physical Review B **109** 205413 ISSN 2469-9969
- [153] Park C H, Son Y W, Yang L, Cohen M L and Louie S G 2008 Nano Letters **8** 2920–2924 ISSN 1530-6984 URL <https://doi.org/10.1021/nl1801752r>
- [154] Xu Y, Zou J and Jin G 2013 Journal of Physics: Condensed Matter **25** 245301 URL <https://dx.doi.org/10.1088/0953-8984/25/24/245301>
- [155] Yang Y, Roques-Carnes C, Kooi S E, Tang H, Beroz J, Mazur E, Kaminer I, Joannopoulos J D and Soljačić M 2021 (*Preprint* 2110.03550)
- [156] Williams J R, Low T, Lundstrom M S and Marcus C M 2011 Nature Nanotechnology **6** 222–225 ISSN 1748-3395
- [157] Wang T T, Bargiel S, Lardet-Vieudrin F, Wang Y F, Wang Y S and Laude V 2020 Applied Sciences **10**
- [158] Sheffer Y, Queiroz R and Stern A 2022 (*Preprint* 2205.02784)
- [159] Jiang Y, Mao J, Moldovan D, Masir M R, Li G, Watanabe K, Taniguchi T, Peeters F M and Andrei E Y 2017 Nature Nanotechnology **12** 1045–1049 ISSN 1748-3395
- [160] Mladenovic D and Dragoman D 2022 Nanomaterials **12** 529 ISSN 2079-4991
- [161] Khan M A and Leuenberger M N 2014 Physical Review B **90** 075439 ISSN 1550-235X
- [162] Bercieux D, van den Berg T, Ferraro D, Rech J, Jonckheere T and Martin T 2020 Eur. Phys. J. Plus **135**, 811 (2020) (*Preprint* 2007.01021)
- [163] Graef H, Wilmart Q, Rosticher M, Mele D, Banszerus L, Stampfer C, Taniguchi T, Watanabe K, Berroir J M, Bocquillon E, Fève G, Teo E H T and Plaçais B 2019 Nature Communications **10** ISSN 2041-1723
- [164] Zhou X 2021 Physical Review B **104** 125441 ISSN 2469-9969
- [165] Lyu K Y and Li Y X 2024 Solid State Communications **384** 115489 ISSN 0038-1098
- [166] Chen S G, Kong X, Zhang B Y and Gong W J 2024 Physical Review B **109** 165418 ISSN 2469-9969
- [167] Wang H Y 2020 Journal of Physics Communications **4** (2020) 125010 (*Preprint* 2010.08340)
- [168] Feng X, Liu Y, Yu Z M, Ma Z, Ang L K, Ang Y S and Yang S A 2020 Physical Review B **101** 235417 ISSN 2469-9969
- [169] Atteia J and Goerbig M O 2021 Phys. Rev. B **103**, 195413 (2021) (*Preprint* 2102.12438)
- [170] Cáceres-Aravena G, Real B, Guzmán-Silva D, Amo A, Torres L E F F and Vicencio R A 2022 Physical Review Research **4** 013185
- [171] Coutant A, Sivadon A, Zheng L, Achilleos V, Richoux O, Theocharis G and Pagneux V 2021 Physical Review B **103** 224309
- [172] Dietz B and Richter A 2018 Physica Scripta **94** 014002 URL <https://dx.doi.org/10.1088/1402-4896/aaec96>
- [173] Torrent D, Mayou D and Sánchez-Dehesa J 2013 Physical Review B **87** 115143
- [174] Martínez-Argüello A M, Toledano-Marino M P, Terán-Juárez A E, Flores-Olmedo E, Báez G, Sadurní E and Méndez-Sánchez R A 2022 Phys. Rev. A **105**(2) 022826 URL <https://link.aps.org/doi/10.1103/PhysRevA.105.022826>
- [175] Stegmann T, Franco-Villafañe J A, Ortiz Y P, Kuhl U, Mortessagne F and Seligman T H 2017 Physics Letters A **381** 24–29
- [176] Ramírez-Ramírez F, Flores-Olmedo E, Báez G, Sadurní E and Méndez-Sánchez R A 2020 Scientific Reports **10** 10229
- [177] Casteels W, Rota R, Storme F and Ciuti C 2016 Physical Review A **93** 043833
- [178] Majari P, Sadurní E, Setare M R, Franco-Villafañe J A and Seligman T H 2021 Physical Review A **104** 013522 ISSN 2469-9934
- [179] Belopolski I, Xu S Y, Koirala N, Liu C, Bian G, Strocov V N, Chang G, Neupane M, Alidoust N, Sanchez D, Zheng H, Brahlek M, Rogalev V, Kim T, Plumb N C, Chen C, Bertran F, Fèvre P L, Taleb-Ibrahimi A, Asensio M C, Shi M, Lin H, Hoesch M, Oh S and Hasan M Z 2017 Science Advances **3** e150169
- [180] Freeney S E, Slot M R, Gardenier T S, Swart I and Vanmaekelbergh D 2022 ACS Nanoscience Au **2** 198
- [181] Betancur-Ocampo Y and Monsivais G 2024 Physical Review B **110** 115432 ISSN 2469-9969
- [182] Süsstrunk R and Huber S D 2015 Science **349** 47–50
- [183] Bellec M, Kuhl U, Montambaux G and Mortessagne F 2013 Physical Review B **88** 115437
- [184] Drost R, Ojanen T, Harju A and Liljeroth P 2017 Nature Physics **13** 668–671
- [185] Zhang Y C 2024 Scientific Reports **14** ISSN 2045-2322
- [186] Huda M N, Kezilebieke S and Liljeroth P 2020 Physical Review Research **2** 043426
- [187] Barbier M, Peeters F M, Vasilopoulos P and Pereira J M 2008 Phys. Rev. B **77**(11) 115446 URL <https://link.aps.org/doi/10.1103/PhysRevB.77.115446>
- [188] Azcona P M and Downing C A 2021 Scientific Reports **11**
- [189] Jakubský V and Zelaya K 2024 Physical Review B **109** 245406 ISSN 2469-9969
- [190] Orso G and Singh M 2021 (*Preprint* 2112.10188)
- [191] Liu X J, Liu Z X and Cheng M 2013 Physical Review Letters **110** 076401
- [192] Tilleke S, Daumann M and Dahm T 2020 Zeitschrift für Naturforschung A **75** 393–402
- [193] Mukherjee S and Thomson R R 2015 Optics Letters **40** 5443
- [194] Hao L 2023 Materials Science and Engineering: B **293** 116486 ISSN 0921-5107
- [195] Jones D, Mucha-Kruczynski M, Ilie A and Covaci L 2025 Nanoscale **17** 5350–5362 ISSN 2040-3372
- [196] Zhang Y C 2022 (*Preprint* 2205.12337)
- [197] Yang Z, Gao F and Zhang B 2016 Scientific Reports **6** 29202
- [198] Hasan M Z and Kane C L 2010 Reviews of Modern Physics **82** 3045–3067 ISSN 1539-0756
- [199] Asbóth J K, Oroszlány L and Pályi A 2016 A Short Course on Topological Insulators (Springer International Publishing)
- [200] Shen S Q 2017 Topological Insulators (Springer Singapore)
- [201] Mallick A, Chang N, Andreev A and Flach S 2021 (*Preprint* 2108.01845)
- [202] Mizoguchi T, Kuno Y and Hatsugai Y 2021 Phys. Rev. B **104**, 035161 (2021) (*Preprint* 2103.03489)
- [203] Ogata T, Kawamura M and Ozaki T 2021 Phys. Rev. B **103**, 205119 (2021) (*Preprint* 2103.10019)
- [204] Katsura H, Kawashima N, Morita S, Tanaka A and Tasaki H 2021 (*Preprint* 2102.10977)
- [205] Mallick A, Chang N, Maimaiti W, Flach S and Andreev A 2020 Phys. Rev. Research **3**, 013174 (2021)

- (Preprint 2009.02881)
- [206] Goerbig M O 2011 *Reviews of Modern Physics* **83** 1193–1243 ISSN 1539-0756
- [207] Pereira V M, Castro Neto A H and Peres N M R 2009 *Physical Review B* **80** 045401 ISSN 1550-235X
- [208] Papaconstantopoulos D A, Mehl M J, Erwin S C and Pederson M R 1997 *MRS Proceedings* **491** ISSN 1946-4274
- [209] Taghizadeh Sisakht E, Zare M H and Fazileh F 2015 *Physical Review B* **91** 085409 ISSN 1550-235X
- [210] Polini M, Guinea F, Lewenstein M, Manoharan H C and Pellegrini V 2013 *Nature Nanotechnology* **8** 625–633
- [211] Palmer S J and Giannini V 2020 *Phys. Rev. Research* **3**, 022013 (2021) (Preprint 2009.07033)
- [212] Hanafi H, Menz P and Denz C 2021 (Preprint 2111.03507)
- [213] Nakatsugawa K and Hu X 2024 *Optics Continuum* **3** 513 ISSN 2770-0208
- [214] Reisner M, Bellec M, Kuhl U and Mortessagne F 2021 *Optical Materials Express* **11** 629
- [215] Kim M and Rho J 2020 *Nanophotonics* **9** 3227–3234
- [216] Tang G J, He X T, Shi F L, Liu J W, Chen X D and Dong J W 2022 *Laser and Photonics Reviews* **16** 2100300
- [217] Martínez-Argüello A M, Toledano-Marino M P, Terán-Juárez A E, Flores-Olmedo E, Báez G, Sadurní E and Méndez-Sánchez R A 2022 *Physical Review A* **105** 022826 ISSN 2469-9934
- [218] Betancur-Ocampo Y, Manjarrez-Montañez B, Martínez-Argüello A M and Méndez-Sánchez R A 2024 *Physical Review B* **109** 104111 ISSN 2469-9969
- [219] Betancur-Ocampo Y, Majari P, Espitia D, Leyvraz F and Stegmann T 2021 *Phys. Rev. B* **103**(15) 155433 URL <https://link.aps.org/doi/10.1103/PhysRevB.103.155433>
- [220] Naumis G G, Barraza-Lopez S, Oliva-Leyva M and Terrones H 2017 *Reports on Progress in Physics* **80** 096501 URL <https://doi.org/10.1088/1361-6633/aa74ef>
- [221] Díaz-Bautista E and Betancur-Ocampo Y 2020 *Phys. Rev. B* **101**(12) 125402 URL <https://link.aps.org/doi/10.1103/PhysRevB.101.125402>
- [222] Díaz-Bautista E 2020 *Journal of Mathematical Physics* **61** 102101
- [223] Pereira V M and Castro Neto A H 2009 *Phys. Rev. Lett.* **103**(4) 046801 URL <https://link.aps.org/doi/10.1103/PhysRevLett.103.046801>
- [224] Ezawa M 2014 *New Journal of Physics* **16** 115004 ISSN 1367-2630
- [225] Midtvedt D, Lewenkopf C H and Croy A 2017 *Journal of Physics: Condensed Matter* **29** 185702 ISSN 1361-648X
- [226] Rudenko A N and Katsnelson M I 2014 *Physical Review B* **89** 201408 ISSN 1550-235X
- [227] Castro Neto A H, Guinea F, Peres N M R, Novoselov K S and Geim A K 2009 *Reviews of Modern Physics* **81** 109–162 ISSN 1539-0756
- [228] Dey B and Ghosh T K 2019 *Physical Review B* **99** 205429
- [229] Thatcher L, Fairfield P, Merlo-Ramírez L and Merlo J M 2022 *Physica Scripta* 035702
- [230] Shen X, Zhu Y Q and Li Z 2022 (Preprint 2201.12628)
- [231] Manjarrez-Montañez B, Méndez-Sánchez R, Betancur-Ocampo Y and Martínez-Argüello A 2025 *International Journal of Solids and Structures* **320** 113435 ISSN 0020-7683
- [232] Walker J S and Gathright J 1994 *American Journal of Physics* **62** 408–422 (Preprint <https://doi.org/10.1119/1.17541>) URL <https://doi.org/10.1119/1.17541>
- [233] Carrera-Escobedo V, Suárez-López J, Martínez-Orozco J, Madrigal-Melchor J and Rodríguez-Vargas I 2014 *Physica E: Low-dimensional Systems and Nanostructures* **63** 248–258 ISSN 1386-9477 URL <https://www.sciencedirect.com/science/article/pii/S1386947714002240>
- [234] Xu Y, He Y and Yang Y 2015 *Physica B: Condensed Matter* **457** 188 – 193 ISSN 0921-4526 URL <http://www.sciencedirect.com/science/article/pii/S0921452614007881>
- [235] Phan A L and Le D N 2021 *The European Physical Journal B* **94**
- [236] Díaz-Bautista E, Betancur-Ocampo Y and Raya A 2024 *Journal of Applied Physics* **136** ISSN 1089-7550
- [237] Carrillo E A, Monsivais G and Flores J A 2021 *physica status solidi (b)* **258** 2100065
- [238] García-Cervantes H, Madrigal-Melchor J, Martínez-Orozco J and Rodríguez-Vargas I 2015 *Physica B: Condensed Matter* **478** 99–107 ISSN 0921-4526 URL <https://www.sciencedirect.com/science/article/pii/S0921452615302222>
- [239] García-Cervantes H, López-Becerra A, Rodríguez-González R and Rodríguez-Vargas I 2022 *Physica B: Condensed Matter* **640** 414052 ISSN 0921-4526 URL <https://www.sciencedirect.com/science/article/pii/S0921452622003659>
- [240] Rodríguez-Vargas I, Madrigal-Melchor J and Oubram O 2012 *Journal of Applied Physics* **112** 073711 (Preprint <https://doi.org/10.1063/1.4757591>) URL <https://doi.org/10.1063/1.4757591>
- [241] Ando T, Nakanishi T and Saito R 1998 *Journal of the Physical Society of Japan* **67** 2857–2862 ISSN 1347-4073
- [242] Ando T 2000 *Semiconductor Science and Technology* **15** R13–R27 ISSN 1361-6641
- [243] Jakubský V, Nieto L M and Plyushchay M S 2011 *Physical Review D* **83** 047702 ISSN 1550-2368
- [244] Jakubský V 2015 *Physical Review D* **91** 045039 ISSN 1550-2368
- [245] Su W P, Schrieffer J R and Heeger A J 1979 *Physical Review Letters* **42** 1698–1701
- [246] Heeger A J, Kivelson S, Schrieffer J R and Su W P 1988 *Reviews of Modern Physics* **60** 781–850
- [247] Meier E J, An F A and Gadway B 2016 *Nature Communications* **7** 13986
- [248] Li X, Meng Y, Wu X, Yan S, Huang Y, Wang S and Wen W 2018 *Applied Physics Letters* **113** 203501
- [249] Lieu S 2018 *Physical Review B* **97** 045106
- [250] Qian K, Zhu L, Ahn K H and Prodan C 2020 *Phys. Rev. Lett.* **125**, 225501 (2020) (Preprint 2005.06450)
- [251] Hu Y, Guo Z X, Zhong Z M and Li Z 2020 *Chinese Physics B* **29** 110302
- [252] Mukherjee A, Nandy A, Sil S and Chakrabarti A 2021 (Preprint 2111.06347)
- [253] Li C A, Choi S J, Zhang S B and Trauzettel B 2022 *Physical Review Research* **4** 023193
- [254] Manda B M, Achilleos V, Richoux O, Skokos C and Theocharis G 2023 *Physical Review B* **107** 184313
- [255] Zhang S H and Yang W 2019 *New Journal of Physics* **21** 103052 ISSN 1367-2630

- [256] Chen S G, Zhang B Y, Yang Z W and Gong W J 2023 Physical Chemistry Chemical Physics **25** 23836–23846 ISSN 1463-9084
- [257] Zhou X 2019 Physical Review B **100** 195139 ISSN 2469-9969
- [258] Cserti J, Pályi A and Péterfalvi C 2007 Physical Review Letters **99** 246801 ISSN 1079-7114
- [259] Lizarraga-Brito J A, Arciniega-Gutiérrez A, Betancur-Ocampo Y and Stegmann T 2025 Physical Review B **112** ISSN 2469-9969
- [260] Lamas-Martínez K J, Briones-Torres J A, Molina-Valdovinos S and Rodríguez-Vargas I 2024 Physical Review B **109** 035416 ISSN 2469-9969
- [261] Du R, Liu M H, Mohrmann J, Wu F, Krupke R, von Löhneysen H, Richter K and Danneau R 2018 Physical Review Letters **121** 127706 ISSN 1079-7114
- [262] Varlet A, Liu M H, Krueckl V, Bischoff D, Simonet P, Watanabe K, Taniguchi T, Richter K, Ensslin K and Ihn T 2014 Physical Review Letters **113** 116601 ISSN 1079-7114
- [263] Dell’Anna L, Majari P and Setare M R 2018 Journal of Physics: Condensed Matter **30** 415301 ISSN 1361-648X
- [264] Biswas R and Sinha C 2021 Scientific Reports **11** ISSN 2045-2322
- [265] Lamas-Martínez K J, Briones-Torres J A, Molina-Valdovinos S and Rodríguez-Vargas I 2023 Physical Review B **107** 245427 ISSN 2469-9969
- [266] Ye X, Ke S S, Du X W, Guo Y and Lü H F 2020 Journal of Low Temperature Physics **199** 1332–1343
- [267] Korol A M, Sokolenko A I and Shevchenko O 2021 Low Temperature Physics **47** 300–305
- [268] Weekes N, Iurov A, Zhemchuzhna L, Gumbs G and Huang D 2021 Physical Review B **103** 165429
- [269] Cheng X, Zhou B, Zhou B and Zhou G 2021 Journal of Physics: Condensed Matter **33** 215301
- [270] Wu Y R and Zhang Y C 2021 Chinese Physics B **30** 060306
- [271] Li F, Zhang Q and Chan K S 2022
- [272] Singh J, Jakhar M and Kumar A 2022 Nanotechnology
- [273] Saleem L, Abdullah H M, Schwingenschlögl U and Manchon A 2025 Physical Review B **111** 024416 ISSN 2469-9969
- [274] Wang J J and Wang J 2025 Journal of Physics: Condensed Matter **37** 255301 ISSN 1361-648X
- [275] Setare M and Jahani D 2010 Physica B: Condensed Matter **405** 1433–1436 ISSN 0921-4526
- [276] Witten E 1981 Nuclear Physics B **188** 513–554 ISSN 0550-3213
- [277] Cooper F, Khare A and Sukhatme U 1995 Physics Reports **251** 267–385 ISSN 0370-1573
- [278] Matveev V B and Salle M A 1991 Darboux Transformations and Solitons (Springer Berlin Heidelberg) ISBN 9783662009222
- [279] Correa F, Inzunza L and Jakubský V 2025 Physical Review Research **7** ISSN 2643-1564
- [280] Nieto L, Pecheritsin A and Samsonov B F 2003 Annals of Physics **305** 151–189 ISSN 0003-4916
- [281] Pecheritsyn A A, Pozdeeva E O and Samsonov B F 2005 Russian Physics Journal **48** 365–374 ISSN 1573-9228
- [282] Zhang P, Wang C, Li Y X, Zhai L and Song J 2023 New Journal of Physics **25** 113021 ISSN 1367-2630
- [283] Andrade E, Carrillo-Bastos R, Asmar M M and Naumis G G 2022 Physical Review B **106** 195413 ISSN 2469-9969
- [284] Ding Z, Wang D, Tao Y and Li M 2023 Physical Review B **108** 245420 ISSN 2469-9969
- [285] Santacruz A, Iglesias P E, Carrillo-Bastos R and Mireles F 2022 Physical Review B **105** 205405 ISSN 2469-9969
- [286] Andrade E, Carrillo-Bastos R and Naumis G G 2025 Journal of Physics: Condensed Matter **37** 193003 ISSN 1361-648X
- [287] Gamayun O V, Ostroukh V P, Gnezdilov N V, Adagideli I and Beenakker C W J 2018 New Journal of Physics **20** 023016 ISSN 1367-2630
- [288] Gao Z and Lan Z 2020 Phys. Rev. B **102**, 245133 (2020) (*Preprint* 2008.10738)
- [289] Fillion-Gourdeau F, Lorin E, MacLean S and Yang X 2025 Journal of Physics A: Mathematical and Theoretical **58** 115302 ISSN 1751-8121
- [290] Stander N, Huard B and Goldhaber-Gordon D 2009 Physical Review Letters **102** 026807 ISSN 1079-7114
- [291] Yu G, Xia J, Lai L, Peng T, Zhu H, Jiang C and Li Y 2023 International Journal of Mechanical Sciences **253** 108412 ISSN 0020-7403
- [292] Dong J, Juričić V and Roy B 2021 Physical Review Research **3** 023056 ISSN 2643-1564
- [293] Lee C H, Imhof S, Berger C, Bayer F, Brehm J, Molenkamp L W, Kiessling T and Thomale R 2018 Communications Physics **1** ISSN 2399-3650
- [294] Albooyeh M R, Sadeghi A and Mohseni S M 2023 Scientific Reports **13** ISSN 2045-2322
- [295] Schäfer F, Fukuhara T, Sugawa S, Takasu Y and Takahashi Y 2020 Nature Reviews Physics **2** 411–425
- [296] Boudjada N, Buessen F L and Paramakanti A 2020 Phys. Rev. B **103**, 165408 (2021) (*Preprint* 2012.07847)
- [297] Segev M and Bandres M A 2020 Nanophotonics **10** 425–434
- [298] Poblete R A V 2021 Advances in Physics: X **6** 1878057
- [299] Yang Y, Lu J, Yan M, Huang X, Deng W and Liu Z 2020 Phys. Rev. Lett. **126**, 156801 (2021) (*Preprint* 2012.14616)
- [300] Laforge N, Wiltshaw R, Craster R V, Laude V, Martínez J A I, Dupont G, Guenneau S, Kadic M and Makwana M P 2020 (*Preprint* 2012.08014)
- [301] Ma T X, Fan Q S, Zhang C and Wang Y S 2021 Journal of Applied Physics **129** 145104
- [302] Wilmart Q, Berrada S, Torrin D, Hung Nguyen V, Fève G, Berroir J M, Dollfus P and Plaçais B 2014 2D Materials **1** 011006 ISSN 2053-1583